



Interaction of ascending magma with pre-existing crustal fractures in monogenetic basaltic volcanism: an experimental approach

Nicolas Le Corvec, Thierry Menand, Jan Lindsay

► To cite this version:

Nicolas Le Corvec, Thierry Menand, Jan Lindsay. Interaction of ascending magma with pre-existing crustal fractures in monogenetic basaltic volcanism: an experimental approach. *Journal of Geophysical Research*, 2013, 118, pp.968-984. 10.1002/jgrb.50142 . hal-00855253

HAL Id: hal-00855253

<https://hal.science/hal-00855253>

Submitted on 6 Sep 2013

HAL is a multi-disciplinary open access archive for the deposit and dissemination of scientific research documents, whether they are published or not. The documents may come from teaching and research institutions in France or abroad, or from public or private research centers.

L'archive ouverte pluridisciplinaire **HAL**, est destinée au dépôt et à la diffusion de documents scientifiques de niveau recherche, publiés ou non, émanant des établissements d'enseignement et de recherche français ou étrangers, des laboratoires publics ou privés.

1 Interaction of ascending magma with pre-existing crustal fractures in
2 monogenetic basaltic volcanism: an experimental approach

3
4 Nicolas Le Corvec¹, Thierry Menand^{2,3,4}, Jan Lindsay¹

5 ¹ School of Environment, The University of Auckland, Private Bag 92019, Auckland 1142, New
6 Zealand. E-mail: n.lecorvec@auckland.ac.nz

7 ² Clermont Université, Université Blaise Pascal, Laboratoire Magmas et Volcans, BP 10448, F-63000
8 Clermont-Ferrand, France

9 ³ CNRS, UMR 6524, LMV, F-63038 Clermont-Ferrand, France

10 ⁴ IRD, R 163, LMV, F-63038 Clermont-Ferrand, France

Abstract

Magma transport through dikes is a major component of the development of monogenetic volcanic fields. These volcanic fields are characterized by numerous volcanic centers, each typically resulting from a single eruption. Therefore magma must be transported from source to surface at different places, which raises the question of the relative importance of 1) the self-propagation of magma through pristine rock, and 2) the control exerted by pre-existing fractures. To address this issue, we have carried out a series of analogue experiments to constrain the interaction of a propagating dike with pre-existing fractures. The experiments involved the injection of air into an elastic gelatin solid, which was previously cut into its upper part to simulate pre-existing fractures. The volume of the dikes, their distance from the fractures and the ambient stress field were systematically varied to assess their influence on potential dike-fracture interactions. The results show that distance and angle between dikes and fractures influence these interactions and the dike trajectory. Dike geometry and dynamics are also affected by both the presence of the fractures and the dike volume; dikes propagating in between fractures tend to decelerate. In nature, interactions are expected for dikes and fractures separated by less than about 200 m, and dikes with a volume less than about 10^{-2} km³ would experience a velocity decrease. These results highlight the influence of pre-existing fractures on the mechanics and dynamics of dikes. These heterogeneities must be considered when studying the transport of magmas within the crust.

Keywords: Dike propagation – Pre-existing crustal fracture – Stress field – Monogenetic basaltic volcanism – Analogue modeling

1 Introduction

Volcanic eruptions are the results of the propagation of magma from source to surface. Geochemical and petrological data from the resulting erupted material provide insights on the source, and the

evolution of the magma during both transfer through and storage within the lithosphere [Zellmer and Annen, 2008]. However, the physical and mechanical understanding of the propagation of a magma-filled crack, or dike, and its relationship with the location and volume of an eruption are still a challenging puzzle [Taisne and Jaupart, 2009; Taisne and Tait, 2009; 2011].

The formation and development of monogenetic basaltic volcanic fields are useful examples of the complexity of magma propagation in the lithosphere. Although monogenetic basaltic volcanic fields occur worldwide, they are most common within extensional regimes [Takada, 1994]. In addition, every field, independent of its tectonic environment, is characterized by numerous volcanic centers showing clustering and lineaments [Connor, 1990; Connor et al., 1992; Mazzarini and D'Orazio, 2003; Mazzarini et al., 2010; Le Corvec et al., Submitted]. Each volcanic center typically results from a single main eruption with magma transported from the mantle, its principal source, to different places on the surface with erupted volumes ranging from 10^{-5} to 1 km^3 of magma (Table 1).

Transport of magma in monogenetic basaltic volcanism is considered to occur via magma-filled cracks, or dikes [Valentine and Hirano, 2010]. Dike propagation starts when the magma pressure in the source is large enough to fracture rocks [Valentine and Hirano, 2010]. Then, as a dike grows and propagates, its buoyancy overcomes the source pressure as the driving mechanism [Menand and Tait, 2002]. The propagation is then driven by the difference between magma and matrix density, or buoyancy, the elastic stress in response to the deformation of the host, and the magma overpressure (the magma pressure in excess of the lithostatic and any potential deviatoric crustal stress acting normally on the dike). On the other hand, dike propagation is restricted by the fracture toughness of the host rocks [Rubin, 1993], and the viscous pressure drop from the flow of magma [Roper and Lister, 2007]. The stress field can either promote extrusive or intrusive growth [Ida, 1999]. Indeed, because a dike is considered as a tensile crack (opening perpendicular to σ_3), the stress field will influence the propagation direction and opening of the dike [Anderson, 1951; Menand et al., 2010] and therefore the possibility of having alignment of volcanic centers at the

surface [Rooney *et al.*, 2011]. However dikes are not passive features, but instead influence their surrounding near-field stress conditions by generating local compressive and extensive stress areas [Roman, 2005; Maccaferri *et al.*, 2010] (Fig. 1c and d). Additionally, there exists conditions of arrest for the vertical propagation of a dike in the upper crust, e.g. level of neutral buoyancy, presence of stratification and the volume of magma within the dike [Taisne *et al.*, 2011a], which may change a vertical propagating dike into a horizontal propagating sill [Kavanagh *et al.*, 2006; Maccaferri *et al.*, 2010; Menand *et al.*, 2010] and thus prevent magma to reach the surface.

The upper part of the lithosphere is known to be brittle and highly fractured [Ranalli, 1995], with pre-existing crustal fracture distributions that are scale independent and follow power laws [Bonnet *et al.*, 2001]. Dikes and crustal fractures are common in the crust; however how they interact is not obvious. Delaney *et al.* [1986] suggested that dikes could either follow self-generated fractures or use pre-existing joints depending on their orientation and magma overpressure. Recent studies show that magmatic intrusions interact with crustal pre-existing fractures (PFs) [Valentine and Krogh, 2006; Gaffney *et al.*, 2007; Wetmore *et al.*, 2009], given certain conditions: i) PFs are almost perpendicular to the least compressive stress σ_3 and steeply dipping ($>60^\circ$); ii) shear stresses on the fracture are small compared to the excess magma pressure; iii) effective ambient dike-normal stress is small compared to the rock tensile strength [Ziv *et al.*, 2000; Valentine and Krogh, 2006; Gaffney *et al.*, 2007]. Additionally, a recent study has shown the strong influence of a PF on the stress field associated with a pressurized magma chamber, and that the position of faults greatly influences the propagation of a dike [Simakin and Ghassemi, 2010].

Pre-existing fractures in the brittle upper crust therefore influence the propagation of magmas as well as the development of monogenetic basaltic fields. This is illustrated in Fig. 1, which shows a dike that cross-cut sedimentary layers and propagated parallel to the dip of the surrounding pre-existing fractures. However, what controls whether a dike interacts with or is influenced by a PF remains an important gap in our understanding of monogenetic basaltic volcanism. Because field

data provide limited information on the dynamics of dike propagation, we studied the interaction between dikes and PFs through analogue modeling. We limited our analysis to the following parameters, considered to influence the interaction between a dike and a PF: 1) the volume of injected magma, 2) the distance between a dike and a PF, and 3) the impact of a deviatoric stress.

Here we show the observations and results of scaled analogue experiments, which aim to constrain the effect of the direction of propagation, shape and velocity of a dike on a potential interaction with PFs. These results are then discussed and related to natural cases.

2 Analogue modelling

The behavior of a buoyant dike and its interaction with PFs in hydrostatic and extensional stress fields were both studied by injecting air in a homogeneous gelatin pre-cut by one or several fractures. Gelatin is a good analogue material having elastic and brittle behavior if prepared properly [Mezger, 2002; Di Giuseppe *et al.*, 2009; Kavanagh *et al.*, 2012]. Indeed, gelatin shows a gradual change in behavior from a purely elastic to visco-elastic rheology in the solid-state to purely viscous rheology in the non-solid-state, depending on its composition, concentration, temperature, ageing and the applied strain state [Di Giuseppe *et al.*, 2009]. Following a preparation as specified by Kavanagh *et al.* [2012], the gelatin in our setup was considered to be an ideal-elastic medium in its solidified state, such that:

$$\sigma = E \cdot \varepsilon \quad (1)$$

where σ is stress, E is the solid Young's Modulus and ε is strain (Hooke's law). These rheological characteristics of the gelatin solids are used to simulate the Earth's upper crust, which behaves, as a

whole, in an elastic way for instantaneous applied stress [Ranalli, 1995]. We used air as an analogue fluid for a buoyantly rising basaltic magma.

2.1 Methodology

Every experiment was carried out using the same set-up. A square-base tank (base: 40 cm x 40 cm, height: 30 cm) was used to create the gelatin block. The tank was made of Perspex, and its base had a series of injection points of 5mm diameter every centimeter from the middle of the tank outward. The gelatin (a high-clarity, 260 bloom, acid, pigskin-derived gelatin) was prepared by mixing gelatin powder with hot water in the tank. Metal plates were introduced on two parallel sides of the tank (Fig. 2a). The gelatin was covered by a thin layer of oil to avoid evaporation during cooling and placed in a fridge at 10°C for 24 hours to allow its solidification.

Once set, the properties of the gelatin were measured as follows. The Young's modulus (E) was calculated by measuring the vertical deflection of the gelatin surface (w) induced by a cylindrical weight of known mass (M) and radius (a) [Timoshenko and Goodier, 1970]:

$$E = \frac{Mg(1-\nu^2)}{2aw} \quad (2)$$

g is the gravitational acceleration, and ν is the gelatin Poisson's ratio ($\nu = 0.5$; Crisp, 1952; Richards Jr and Mark, 1966). The fracture toughness (K_c) was then calculated using the relationship derived by Kavanagh et al. [2012]:

$$K_c = (1.4 \pm 0.1) \sqrt{E} \quad (3)$$

In some experiments, PFs were created, after the Young's modulus had been measured, by cutting the upper part of the gelatin using a rail-guided knife (9 cm deep). Then, before starting an experiment, both metal plates (12 mm thick) were removed and replaced by cold water to create free surface conditions on each side of the gelatin (Fig. 2b and c). To create an extensional regime, the gelatin was first unstuck from the three other sides (front, back and bottom side) of the tank to ensure the extension to be homogeneous throughout the gelatin solid (Figs. 2 and 3). Then a horizontal tensile deviatoric stress was created by imposing a homogeneous, vertical compressive load on its entire upper surface (Fig. 2c), as detailed in section 2.3. Finally, a pre-cut of a few millimeters was made at the base of the gelatin solid before injecting air in order to force the experimental dike (referred in the following as dike) to propagate perpendicularly to the front side of the tank or, for some experiments, parallel to the plane of the PF(s). A predetermined volume of air was injected inside the gelatin through the injection points using a syringe, which allowed us to control and vary the volume of injected air from one experiment to another. Each experiment was recorded using a digital video camera. The movies were subsequently analyzed using a MATLAB script to measure the evolution of the shape, the direction of propagation and the velocity of the dike inside the gelatin (See Appendix 1). The pictures were analyzed from the moment the dike was separated from the syringe until it reached the surface. This analysis allowed us to determine any potential impact of PF on the dike propagation.

2.2 Scaling

Analogue models are used to identify and analyze the main processes operating in natural systems at the laboratory scale [Ramberg, 1981]. The analogue model of the Earth should be geometrically, kinematically and dynamically similar to its natural prototype [Hubbert, 1937]. Here we follow the scaling procedure for analogue intrusions detailed by Kavanagh et al. [2012].

Our experiments consider the propagation of a buoyant magma-filled crack through an elastic medium, thus our setting must create a density contrast (i.e., buoyancy) and a resistance to the fracturing of the medium (i.e., fracture toughness) similar to those existing in the Earth's crust.

Our experiments consider the propagation of a buoyant magma-filled crack through an elastic medium resisted by the fracture resistance of the medium. The balance between these two forces takes place near the tip of the dike over the buoyancy length scale Lb , where:

$$Lb = \left(\frac{K_c}{\Delta \rho g} \right)^{2/3} \quad (4)$$

and $\Delta \rho$ is the difference between the density of the solid and that of the fluid, g is the gravitational acceleration, and K_c is the fracture toughness of the solid [Taisne and Tait, 2009]. This buoyancy length, Lb , corresponds to the minimum dike length needed for fracturing the surrounding rocks, and it occurs when the stress intensity factor at the dike tip K_I equals the rock fracture toughness K_c [Menand and Tait, 2002].

To scale our experiments geometrically, we calculated the ratio (Lb^*) between the buoyancy length of the intrusion in our model (Lb_m) and that in nature (Lb_n):

$$Lb^* = \frac{Lb_m}{Lb_n} = \left(\frac{K_{c_m} \Delta \sigma_m}{K_{c_n} \Delta \sigma_n} \right)^{2/3} \quad (5)$$

In our experiments, $\Delta \rho = \rho_{gelatin} = 1000 \text{ kg/m}^3$ and the gelatin mean fracture toughness $K_c \sim 70 - 80 \text{ Pa.m}^{1/2}$ (Table 3). Taking a density difference between rocks and magma $\Delta \rho = 100 \text{ kg/m}^3$ and a

fracture toughness $K_c = 10^7 \text{ Pa.m}^{1/2}$ as representative values for a basaltic volcanic field, we find that, for our experiments, the ratio $Lb^* \sim 10^{-4}$. Our model is then $\sim 10^4$ smaller than the natural system and thus represents a shallow portion of crust, namely the upper 2-3 km. The natural dimensions represented by our model are listed in Table 2. The scaled volume injected in our experiments lies in the range of volume erupted in monogenetic volcanic fields (Table 1).

Likewise, the time scale in our experiments differs from that in nature, and our experiments must be scaled kinematically. We scaled our experimental velocities using the reduced gravity g' [Shankar Subramanian, 1992], which is the effective gravitational acceleration in the host solid due to buoyancy forces:

$$g' = \frac{\Delta\rho}{\rho_{solid}} g \quad (6)$$

where

$$\Delta\rho = \rho_{solid} - \rho_{air} \quad (7)$$

Combining g' with Lb , we found the time scale

$$T = \sqrt{Lb/g'} \quad (8)$$

195 which allows us to calculate the velocity scale

196

$$197 \quad U = Lb/T \quad (9)$$

198

$$199 \quad U = (\Delta\rho g)^{\frac{1}{6}} Kc^{\frac{1}{3}} \rho_{solid}^{-\frac{1}{2}} \quad (10)$$

200

201 or

202

$$203 \quad U = \left(\frac{Kc}{\rho_{solid}} \right)^{\frac{1}{3}} g'^{\frac{1}{6}} \quad (11)$$

204

205 A kinematic scaling ratio U^* can therefore be calculated:

206

$$207 \quad U^* = \frac{U_{model}}{U_{nature}} \quad (12)$$

208

209 Using the same representative natural values of density difference and fracture toughness as before,

210 and taking a rock density of 2500 kg/m³, equation (12) gives a kinematic scaling ratio $U^* = 0.046$.

211 Propagation velocities in our model (mean value= ~13.10⁻³ m/s) are therefore in accordance with

212 basaltic dike velocities in nature (0.1-1 m/s) [Taisne et al., 2011b].

213 2.3 Stress regimes

214 We investigated two different stress regimes with our experiments.

215 2.3.1 Hydrostatic regime

216 In this set of experiments, no deviatoric stresses were applied to the gelatin (Fig. 2b). Because the
217 gelatin is considered as a pure elastic medium with a Poisson's ratio $\nu = 0.5$, the state of stress in the
218 gelatin at the start of an experiment is hydrostatic [Takada, 1990] and references therein):

219

$$220 \quad \sigma_x = \sigma_y = \sigma_z \quad (13)$$

221

222 2.3.2 Extensional regime

223 In this set of experiments, a horizontal tensile deviatoric stress was applied. Because of the weak
224 tensile strength of the gelatin, this was done by imposing a load on the upper surface of the gelatin.
225 Since the gelatin was constrained by two opposite tank walls, in the Y-direction, as well as the rigid
226 base of the tank, the gelatin was only free to move in the other X-direction (Fig. 2c). This horizontal
227 deformation of the gelatin solid obtained by imposing a vertical positive compressive deviatoric
228 stress σ_z , and thus a negative compressive strain ε_z is identical to the horizontal deformation that
229 would have been created by imposing the (negative) tensile horizontal deviatoric stress σ_x :

230

$$231 \quad \varepsilon_x = -\varepsilon_z = \frac{3}{4} \left(\frac{\sigma_z}{E} \right) \quad (14)$$

232

$$233 \quad \varepsilon_x = -\varepsilon_z = \frac{3}{4} \left(\frac{-\sigma_x}{E} \right) \quad (15)$$

234

2.4 Limitations

Because natural systems are complex systems, their modeling requires simplifications. We assume our homogeneous solid with brittle – elastic behavior to represent the upper couple of kilometers of the crust. However, the crust is not homogeneous, and layering may influence dike direction [Gudmundsson, 2005; Taisne and Jaupart, 2009; Maccaferri et al., 2010], which could have an important impact on the interaction of a dike with PFs. We neglected layering and heterogeneities to focus only on the PFs and their potential effect on dike propagation.

In our experiments, we neglect viscous forces, which may play an important role in the dike dynamics [Lister and Kerr, 1991], and assume instead that fracturing of the host solid controls the dynamics of the dikes. By injecting constant volumes of air as an analogue for magma, we create buoyancy-driven dikes with constant volume, whereas in nature the viscosity of magma prevents the complete extraction of the liquid from the dike tail [Stevenson, 1982; Taisne and Tait, 2009]. However, the propagation of buoyant dikes is controlled by the local buoyancy balance that takes place at the dike nose region [Lister and Kerr, 1991]. Finally, we assume that magma heat loss is negligible during the propagation of mafic dikes due to their high velocity (up to meters per second: [Demouchy et al., 2006]), which is a reasonable assumption for basaltic dikes greater than a meter in thickness [Bruce and Huppert, 1989].

3 Observations and results

In every experiment, a pre-defined volume of air is injected at the bottom of the tank using a syringe. The experimental dike grows initially as a penny-shaped crack until the dike reaches a certain height, i.e. its buoyancy length (L_b). From that point, the tip of the dike is able to fracture the gelatin leading to its upward propagation. Once all the volume of air is injected, the dike breaks loose from the syringe and propagates vertically, keeping its volume constant by opening at its tip and closing at its tail within the gelatin. The dikes were injected so that they propagated vertically in

a plane parallel to the camera axis. However, their orientation could be either parallel or perpendicular to the PFs.

3.1 Observations

3.1.1 No pre-existing fracture

In the experiments with no PFs, we observed vertical to sub-vertical directions of propagation without any noticeable changes in the shape of the experimental dike while propagating within the gelatin. We did observed an increase in length and an increase in velocity as the tip of the dike was reaching the surface of the gelatin. These observations fit well with similar experiments done in previous studies (e.g., *Rivalta and Dahm, 2006; Menand et al., 2010*).

3.1.2 One pre-existing fracture

In the experiments with one PF, we observed, as in the experiments without PFs, that the experimental dikes propagated vertically or sub-vertically within the gelatin. We observed in some experiments that the dike interacted with the PF. Whether a dike interacted with a PF depended on the orientation of the dike (parallel or perpendicular to the PF) and of the PF dip (vertical or not) (Fig. 4a and b), as well as the direction of propagation of the dike (vertical or sub-vertical) and its distance from the PF. As soon as the dike touched a PF, its ascent stopped and all the contained air was immediately drained in the PF.

3.1.3 Two pre-existing fractures

In the experiments with 2 PFs, we observed, as in the previous experiments, vertical to sub-vertical directions of propagation of the experimental dike in between the PFs. We also observed that the dikes were channeled in between the PFs, which affected their direction of propagation (Fig. 5, exp 2500). However if the distance between the PFs was too small the dike interacted with one of the PFs (Fig. 5, exp 3000). Also the changes in the direction of propagation were more important when the PFs were sub-parallel to the dike (Fig. 5, exp 2804L, 2900, 2809R and 2811L). Finally, the

influence of the angle between the dike and the PF seemed to play an important role in the interaction (exp 2804L). We observed that a high angle between the dike and the PF enhanced the potentiality of interaction between the two.

3.2 Results

In order to quantify the mechanical parameters potentially controlling the interaction between a dike and a PF (Table 4), we defined three dimensionless values: d^* , D^* and Vol^* .

d^* is the dimensionless distance of the dike from the PF:

$$d^* = \frac{d}{Lb} \quad (16)$$

with d defined as the distance between the tip of the dike and the closest PF, or in the case where the dike interacted with a PF the distance between the tip of the dike and the interacting PF. This distance d was measured when the tip of the dike reached the level of the PF (Fig. 4a).

D^* is the dimensionless distance between 2 PFs:

$$D^* = \frac{D}{Lb} \quad (17)$$

with D defined as the distance between the two PFs that channel a dike (Fig. 5).

Vol^* is a dimensionless dike volume defined as the ratio of the volume of air injected for each experiment, Vol (Table 3) and the buoyancy volume, $Volb$:

$$Volb = 2(1 - \nu^2)\Delta\rho g Lb^4/E \quad (18)$$

305

306 based on the dike buoyancy length Lb :

307

$$Vol^* = \frac{Vol E}{2(1-\nu^2)\Delta\rho g Lb^4} \quad (19)$$

309

310 In the following, we focus first on the mechanical parameters controlling a dike-PF interaction, then
 311 on the influence of the PFs on the shape of the experimental dike, and finally on their effect on the
 312 dynamics of the experimental dike.

313 3.2.1 Mechanical parameters controlling a dike-PF interaction

314 The dimensionless volume of air Vol^* injected and the angle α between the dike and the PF when
 315 the tip of the dike reached the PF level (Fig. 4b) were plotted against d^* and D^* (Fig. 6). First, we
 316 observe that the distance between a dike and a PF (d^*), and the distance between 2 PFs (D^*)
 317 influences the potential interaction between dikes and nearby PFs. According to Fig. 6, dikes interact
 318 with PFs when $d^* < \sim 0.4$ and when $D^* < \sim 0.8$ (exp 3000 in Fig. 5); otherwise dikes are neither
 319 influenced (Fig. 4a) nor channelized by the PFs (exp 2500 in Fig. 5). Fig. 6 shows also that dikes
 320 propagating at a high angle α relative to the PFs favor interaction over larger dimensionless
 321 distances d^* and D^* (Fig. 4b and exp 2804L in Fig. 5) However, we note two exceptions: 1- dikes that
 322 change their direction of propagation (dotted ellipse in Fig. 6 and 7 and exp 2809R and 2811R in Fig.
 323 5), and thus avoid interaction with the PFs; and 2- dikes that were injected closer to one PF in
 324 experiments with 2 PFs (green circle in Fig. 6 and 7) will interact with that PF since $d^* < 0.4$ (Fig. 6a
 325 and 6b). The figures also suggest that the volume and the stress regime do not influence interactions
 326 between dike and PF.

3.2.2 Influence of the pre-existing fracture on the shape of the experimental dike

The length and the thickness of the experimental dike were extracted using the digital video records. We extracted the average length (L_b) and the thickness (t_b) of the experimental dike once it broke loose from the syringe until it reached the level of the PF, and the average length (L_a) and thickness (t_a) after that level but before the last final acceleration due to the free surface (Table 4). We then calculated the difference in length, ΔL , and thickness, Δt , before and after the PF level:

$$\Delta L = L_a - L_b \quad (20)$$

And

$$\Delta t = t_a - t_b \quad (21)$$

Positive values in ΔL and Δt imply an increase in length and thickness of the propagating dikes, respectively, as they crossed the level of the PF.

ΔL and Δt are plotted against each other in Fig. 8, which reveals a correlation between these two parameters: in the majority of experiments the length of the propagating dike decreased due to the presence of PFs while its thickness increased; most dikes got shorter and fatter once they reached the PF level.

In the majority of experiments, the thickness of the dikes increased as the dike passed the PF level irrespective of the number of PFs, the stress regime and whether dike-PF interaction occurred. This thickness increase remains modest, however: the maximum changes in thickness reach ~5%. The

length of the dikes, however, seems to be affected differently depending on the number of PFs. In experiments with a single PF, a similar number of dikes got longer or shorter. This contrasts with experiments involving two PFs, for which, in almost all cases, the propagating dikes shortened ($\Delta L < 0$) as they entered the region flanked by the two PFs. The maximum changes in length reach $\sim 30\%$. Overall, it seems the changes in length and thickness were stronger in experiments involving one single PF.

However, the reason for these changes in length and thickness remains unclear as no noticeable effect of either the distance d^* between dike and PF (Fig. 7a,b), the distance D^* between two PFs (Fig. 7c,d), or the volume Vol^* of air injected (Fig. 7e,f) is observed. The largest decrease in dike length has been observed for $d^* \sim 0.5$ and $D^* \sim 1$, but these only concern a couple of observations for which we cannot detect any associated effect on the dike thickness.

3.2.3 Dynamic aspects

3.2.3.1 No pre-existing fracture

The sequential analysis of the experiments shows that dikes propagate at a constant velocity within the gelatine. As the dikes reach the surface, we observe an acceleration due to the presence of a free surface as demonstrated by Rivalta et al. (2006).

3.2.3.2 With pre-existing fractures

We observed that the presence of PFs could channel propagating dikes (Fig. 5) and that they changed the dikes shape. We now examine whether PFs could also affect their propagation velocity. To do this, we extracted from the digital video records the average velocity v_b of the dikes before they reach the PF level and the average velocity v_a after that level but before the last final acceleration due to the free surface (Table 4). We then calculated the velocity difference before and after the PF level:

$$\Delta V = v_a - v_b \quad (22)$$

374

375 Again, negative values for ΔV means that dikes experience a deceleration as they pass the level of
 376 PFs. In order to analyse these potential velocity changes, ΔV is plotted against d^* , D^* and V^* .

377 The results show that almost all experimental dikes experienced a change in their propagation
 378 velocity, although this change was of small magnitude (Fig. 9). Most dikes show a decrease in
 379 velocity due to the presence of PFs: an increase in velocity ($\Delta V > 0$) is only observed for experiments
 380 with one single PF (up to 3% increase, Fig. 9), whereas experiments involving 2 PFs all resulted in
 381 either no velocity change or a velocity decrease (up to 6% decrease, Fig. 9).

382 The distance separating a dike from a PF seems to have some influence on the velocity as dikes that
 383 propagate closest to PFs tend to experience a velocity increase whereas dikes furthest away
 384 experience the largest velocity decrease (Fig. 9a). Despite some scatter in the results, we also
 385 observe that when a dike propagated between two PFs the distance between these PFs influenced
 386 the dike dynamics. Plotting the difference in velocity of the dike, ΔV , against the dimensionless D^*
 387 value, reveals that the change in velocity induced by the presence of the two PFs is largest when the
 388 PFs are separated by a dimensionless distance $D^* \sim 1$ (Fig. 9b). Our results suggest that PFs that are
 389 too far away from each other cannot influence the velocity of propagating dikes. Likewise, and more
 390 interestingly, PFs that are close to each other ($D^* < 1$) do not seem to influence the dike velocity
 391 either.

392 The injected volume influences also the variation of dike velocity (Fig. 9c). For the experiments with
 393 a single PF, no apparent correlation is observed. On the other hand, when 2 PFs are present we
 394 observe a positive correlation with ΔV , with ΔV becoming even more negative as Vol^* diminishes.
 395 Additionally, we observe that ΔV tends to zero when $Vol^* \sim 1000$, which would suggest that beyond
 396 that threshold the influence of PFs does not affect, or much less, the velocity of ascent of a dike. An

explanation might be that the buoyancy of such dikes is large enough to counter the potential effect of nearby PFs on their dynamics.

The change in the dynamics of the dike induced by the presence of PFs seems to be related to the change in the shape of the dike. Indeed Figure 10a shows a positive correlation, albeit weak, between ΔV and ΔL : any increase (decrease) in dike length is associated with an increase (decrease) in propagation velocity. This correlation is consistent with that identified between ΔV and Vol^* , since larger volumes imply larger dike lengths. A similar correlation is observed between dike thickness and velocity with the larger positive (negative) velocity changes associated with thicker (thinner) dikes (Fig. 10b). Our interpretation is that the presence of PFs affects the shape of dikes propagating nearby, which in turn affects their dynamics. This effect appears more important when dikes propagate in between PFs separated by a dimensionless distance $D^* \sim 1$.

Finally, we note that our experiments do not reveal any potential effect of the stress regime on the dynamics of the PFs.

4 Implications for the interaction of propagating dikes and pre-existing fractures

The experiments show that PFs can influence dikes in several ways.

4.1 Mechanical aspects: implications on fracture density and dike volume

First, if a dike propagates relatively close to a PF, they can interact as shown by Conway et al. [1997] and our experiments (Fig. 4b). If the dike overpressure is higher than the normal stress acting on the PF [Kiyosugi et al., 2010], then the dike will be able to exploit and thus potentially reach the surface. However, our experiments do not distinguish for which conditions the interactions dike-PF are passive, i.e. a dike interacts with a PF simply because it is on the dike path, or active, i.e. the PF influences the trajectory of the propagating dike probably by modifying the local stress field and thus capturing the propagating dike. Our experiments show that these interactions occur when the

dimensionless distance between a dike and a PF is lower than ~ 0.4 , that is when the distance that separates a dike from neighboring PFs is less than about 0.4 its buoyancy length Lb :

$$d < 0.4Lb = 0.4 \left(\frac{K_c}{\Delta \rho g} \right)^{2/3} \quad (23)$$

Thus, the potential for dike-PF interaction depends not only on the density of PFs in a given region of the superficial crust but also on the characteristic length (Lb) of the dikes intruding this crustal region.

The continental crust has an average quartz diorite-type composition, with a density of 2800 kg/m^3 . The values for the elastic moduli $E = 80 \text{ GPa}$ and $\nu = 0.25$ [Turcotte and Schubert, 1982]. The difference in density between a mafic dike and the crust is generally taken as $\Delta \rho = 100 \text{ kg/m}^3$ [Rubin, 1995]. Although taking a single fracture-toughness value for crustal rocks can be debatable [Rubin, 1993], $10 \text{ MPa.m}^{1/2}$ seems a reasonable representative value for the continental crust. The gravitational acceleration g is taken as 9.81 m/s^2 . With these values, our results suggest dike-PF interaction will occur if the distance between a dike and a PF is lower than $\sim 200 \text{ m}$ (eq. 23).

Furthermore, dike-PF interactions are more likely if the strike of the PF differs from that of the dikes, and if the angle between the dike and the PFs is high. Interpretations of volcanic vents alignments in nature have raised questions on their potential controls: 1- the stress field [Nakamura, 1977]; and 2- the pre-existing crustal fractures [Valentine and Krogh, 2006]. Our results suggest that dikes have a greater chance of interaction with crustal PFs formed during a previous, different stress regime because dikes will then tend to propagate at high angles to the PFs. If the stress regime has changed since the PF formation, the alignments do not represent the stress regime during intrusion. Dikes propagate essentially vertically, due to their buoyancy. Faults with low dips are more susceptible to

interact with propagating dikes, as well as normal faults rather than reverse faults because the normal stress acting on normal faults is weaker [Anderson, 1951]. However, the dike still needs to overcome the normal stress acting on the PF in order to intrude it [Delaney *et al.*, 1986] or will only be diverted for a small distance [Gaffney *et al.*, 2007].

Our experiments also suggest that a dike can be channelized in between two adjacent PFs, those modifying the trajectory of the propagating dike. Michon *et al.* [2007] described that at Piton de la Fournaise dikes followed the curved rift system. These authors assumed the edifice modifies the ambient stress field over fairly shallow depths. We can infer from our results that in this scenario the rift zone may in fact have influenced the propagation of a dike by channelizing it parallel to the rift.

Finally, our experiments do not show any evidence for an eventual role of the tectonic regime. No difference has been observed between the hydrostatic stress field and the extensional stress field. We can envisage two possibilities. First, our experimental results could simply reflect a real lack of effect from the stress field on potential interaction between a dike and a PF. However, PFs seem to modify, in certain cases, the dike trajectories. This would therefore suggest a modification and thus an effect of the local stress field. Moreover any stress field will add to the force budget of a dike, which determines its propagation trajectory. Thus this apparent lack of effect of the stress field seems dubious. A second possibility would be that PFs, due to their presence, act as a screen or shield to the remote stress field. A dike propagating in between 2 PFs would thus not feel the difference between the hydrostatic case and the deviatoric case; the latter would be limited to the region outside the PFs. However, this scenario cannot explain the results for our experiments with a single PF.

4.2 Dynamic aspect

In addition to modifying the geometry and trajectory of propagating dikes, PFs affect also their dynamics. The difference in the velocity of a dike before and after the PFs level decreases for most

of the experiments (Fig. 9), although some experiments displayed an acceleration of the dike when only one PF was involved (Fig. 9a). In addition, the volume of the dikes influences the degree of deceleration when the dikes propagate in between two adjacent PFs (Fig. 9c). These variations in velocity are accompanied by variations in the shape of the dike, mainly a decrease in length and an increase in thickness (Fig. 10a and b).

The dynamics of dikes in nature are difficult to analyze because we cannot see dikes directly and the quantitative analysis of their propagation is limited to the potential seismicity generated by their propagation [Battaglia *et al.*, 2005]. Taisne *et al.* 2011b show that the propagation of a dike at Piton de la Fournaise does not occur at a constant velocity but is in fact affected by changes in velocity and periods of arrest. The results suggest the influence of heterogeneities such as layering [Taisne and Jaupart, 2009; Maccaferri *et al.*, 2011; Taisne and Tait, 2011], but could also be due to the presence of PFs as suggested by our results. Our results also show that dikes might not reach the surface if their volumes are too small, since PFs will tend to decelerate their velocity thus increasing the probability for the dikes to stall. On the other hand, PFs will tend to help a dike to reach the surface if it interacts with the PF.

Our results suggest that the dynamics of dikes are affected more when their volume is rather small, especially if they intrude a region with more than one pre-existing fracture. More specifically, for dikes propagating in between two adjacent PFs, only those with a normalized volume Vol^* smaller than ~ 1000 seem to be sensitive to the presence of PFs. Above this threshold, dike dynamics would be rather insensitive to PFs owing to their large volume. Therefore for the dynamics of propagating dikes to be affected by PFs, dike volumes needs to be less than a critical volume Vol_c :

$$Vol < Vol_c = 1000 \frac{2(1-\nu^2)\Delta\rho g L b^4}{E} \quad (24)$$

We can use this expression to estimate this critical volume for dikes in nature. Using the same values as before for the properties of crustal rocks and magmas ($E=10$ GPa, $\nu = 0.25$, $\Delta\rho = 100$ kg/m³ and $K_c = 10$ MPa.m^{1/2}), eq. (24) suggests that dikes with a volume lower than $Vol_c \sim 10^{-2}$ km³ would experience a change in their dynamics, i.e. a decrease in their propagation velocity, induced by the surrounding PFs. This value is well within the range of erupted volumes at various monogenetic basaltic volcanic fields (Table 1), which thus suggests that some of their volcanic centres might have resulted from dike-PFs interactions.

5 Conclusion

Using analogue modelling, the behaviour of a buoyant dike propagating in a homogeneous medium affected by one or several PFs in hydrostatic and extensional stress fields has been investigated and quantified. These experiments show that the presence of PFs influences the shape, the direction of propagation and the dynamic of the dike.

The experiments show that the interaction between a dike and a PF is mainly due to their separating distance, d^* , or the distance separating two PFs, D^* , and the angle, α , between them. However, the results cannot distinguish between an active deviation of the dike trajectory by the PFs and a passive intersection of the PF by the dike. The influence of PFs on the dikes varies depending of the number of PFs. While the presence of a single PF could induce either an increase or a decrease in both dike length and velocity, in experiments with two PFs we observed almost exclusively a decrease in the length and velocity of the dikes. These changes seem to be controlled by the volume of the dike, with the larger changes occurring for smaller volumes. A scaling analysis suggests: 1) that dike-PF interaction in nature is likely to occur when the horizontal distance that separate propagating dikes from nearby PFs becomes less than about 200 m; and 2) that dikes with a volume less than about 10^{-2} km³ would experience a decrease in their propagation velocity owing to the presence of surrounding PFs.

This study shows how the presence of pre-existing crustal fractures can influence the direction of propagation and the dynamics of dikes, and thus helps magma to erupt at different places within a volcanic field. These heterogeneities must therefore be taken in account in further investigations of dike propagation in the upper parts of the lithosphere.

Acknowledgments

We would like to thank the University of Bristol for hosting our project at Geological Fluid Mechanics Lab, in particular Steve Sparks, and the workshop for their help to design and build up the material necessary for the experiments. We also thank Janine Kavanagh, Mikel Diez, Julie Rowland and Kat Daniels for interesting and helpful discussion on the topic. This study was funded by the Determining Volcanic Risk in Auckland (DEVORA) project. This is Laboratory of Excellence *ClerVolc* contribution n° XXX.

References

- Allen, S. R., and I. E. M. Smith (1994), Eruption styles and volcanic hazard in the Auckland volcanic field, New Zealand, *Geoscience Reports - Shizuoka University*, 20, 8-14.
- Anderson, E. M. (1951), *The Dynamics of Faulting and Dyke Formation With Applications to Britain*.
- Battaglia, J., V. Ferrazzini, T. Staudacher, K. Aki, and J.-L. Cheminée (2005), Pre-eruptive migration of earthquakes at the Piton de la Fournaise volcano (Reunion Island), *Geophysical Journal International*, 161(2), 549-558.
- Bonnet, E., O. Bour, N. E. Odling, P. Davy, I. Main, P. Cowie, and B. Berkowitz (2001), Scaling of fracture systems in geological media, *Reviews of Geophysics*, 39(3), 347-383.
- Bruce, P. M., and H. E. Huppert (1989), Thermal control of basaltic fissure eruptions, *Nature*, 342(6250), 665-667.
- Connor, C. B. (1990), Cinder cone clustering in the TransMexican Volcanic Belt: implications for structural and petrologic models, *Journal of Geophysical Research*, 95(B12).
- Connor, C. B., C. D. Condit, L. S. Crumpler, and J. C. Aubele (1992), Evidence of Regional Structural Controls on Vent Distribution: Springerville Volcanic Field, Arizona, *J. Geophys. Res.*, 97.
- Conway, F. M., D. A. Ferrill, C. M. Hall, A. P. Morris, J. A. Stamatakis, C. B. Connor, A. N. Halliday, and C. Condit (1997), Timing of basaltic volcanism along the Mesa Butte Fault in the San Francisco Volcanic Field, Arizona, from ⁴⁰Ar/³⁹Ar dates: Implications for longevity of cinder cone alignments, *J. Geophys. Res.*, 102(B1), 815-824.
- Crisp, J. D. C. (1952), The use of gelatin models in structural analysis, *Proc. Inst. Mech. Eng. Part B*, 1 B(12), 580-604.
- Delaney, P. T., D. D. Pollard, J. I. Ziony, and E. H. McKee (1986), Field relations between dikes and joints: Emplacement processes and paleostress analysis, *Journal of Geophysical Research*, 91(B5), 4920-4938.
- Demouchy, S., S. D. Jacobsen, F. Gaillard, and C. R. Stem (2006), Rapid magma ascent recorded by water diffusion profiles in mantle olivine, *Geology*, 34(6), 429-432.

552 Di Giuseppe, E., F. Funiciello, F. Corbi, G. Ranalli, and G. Mojoli (2009), Gelatins as rock analogs: A
 553 systematic study of their rheological and physical properties, *Tectonophysics*, 473(3-4), 391-403.
 554 Favalli, M., D. Karátson, F. Mazzarini, M. T. Pareschi, and E. Boschi (2009), Morphometry of scoria
 555 cones located on a volcano flank: A case study from Mt. Etna (Italy), based on high-resolution LiDAR
 556 data, *Journal of Volcanology and Geothermal Research*, 186(3-4), 320-330.
 557 Gaffney, E. S., B. Damjanac, and G. A. Valentine (2007), Localization of volcanic activity: 2. Effects of
 558 pre-existing structure, *Earth and Planetary Science Letters*, 263(3-4), 323-338.
 559 Gudmundsson, A. (2005), The effects of layering and local stresses in composite volcanoes on dyke
 560 emplacement and volcanic hazards, *Comptes Rendus Geoscience*, 337(13), 1216-1222.
 561 Hasenaka, T., M.-W. Lee, H. Taniguchi, A. Kitakaze, T. Miyamoto, and H. Fujimaki (1997), Catalogue
 562 of the Volcanoes from the Cheju Monogenetic Volcano Group, Korea, *Northeast Asian Studies*, 2, 41-
 563 74.
 564 Hubbert, M. K. (1937), Theory of scale models as applied to the study of geologic structures,
 565 *Geological Society of America Bulletin*, 48(10), 1459-1519.
 566 Ida, Y. (1999), Effects of the crustal stress on the growth of dikes: Conditions of intrusion and
 567 extrusion of magma, *J. Geophys. Res.*, 104(B8), 17897-17909.
 568 Kavanagh, J. L., T. Menand, and R. S. J. Sparks (2006), An experimental investigation of sill formation
 569 and propagation in layered elastic media, *Earth and Planetary Science Letters*, 245(3-4), 799-813.
 570 Kavanagh, J. L., T. Menand, and K. A. Daniels (2012), Gelatine as a crustal analogue: Determining
 571 elastic properties for modelling magmatic intrusions, *Tectonophysics*, under review.
 572 Kiyosugi, K., C. B. Connor, D. Zhao, L. J. Connor, and K. Tanaka (2009), Relationships between volcano
 573 distribution, crustal structure, and P-wave tomography: an example from the Abu Monogenetic
 574 Volcano Group, SW Japan, *Bulletin of Volcanology*, 1-10.
 575 Kiyosugi, K., A. Takada, K. Tanaka, Y. Miyata, C. B. Connor, and D. Roman (2010), Interaction of dyke
 576 and preexisting fracture suggested by laboratory experiments, *6th International Dyke Conference*,
 577 *Varanasi, India, Abstracts*, 73.
 578 Le Corvec, N., K. B. Spörli, J. V. Rowland, and J. M. Lindsay (Submitted), Spatial distribution and
 579 alignments of volcanic centers: Clues to the formation of monogenetic volcanic fields?, *Earth-Science*
 580 *Reviews*.
 581 Lister, J. R., and R. C. Kerr (1991), Fluid-mechanical models of crack propagation and their application
 582 to magma transport in dykes, *Journal of Geophysical Research*, 96(B6).
 583 Maccaferri, F., M. Bonafede, and E. Rivalta (2010), A numerical model of dyke propagation in layered
 584 elastic media, *Geophysical Journal International*, 180(3), 1107-1123.
 585 Maccaferri, F., M. Bonafede, and E. Rivalta (2011), A quantitative study of the mechanisms governing
 586 dike propagation, dike arrest and sill formation, *Journal of Volcanology and Geothermal Research*,
 587 208(1-2), 39-50.
 588 Mazzarini, F., and M. D'Orazio (2003), Spatial distribution of cones and satellite-detected lineaments
 589 in the Pali Aike Volcanic Field (southernmost Patagonia): insights into the tectonic setting of a
 590 Neogene rift system, *Journal of Volcanology and Geothermal Research*, 125(3-4), 291-305.
 591 Mazzarini, F., L. Ferrari, and I. Isola (2010), Self-similar clustering of cinder cones and crust thickness
 592 in the Michoacan-Guanajuato and Sierra de Chichinautzin volcanic fields, Trans-Mexican Volcanic
 593 Belt, *Tectonophysics*, 486(1-4), 55-64.
 594 Menand, T., and S. R. Tait (2002), The propagation of a buoyant liquid-filled fissure from a source
 595 under constant pressure: An experimental approach, *Journal of Geophysical Research B: Solid Earth*,
 596 107(11).
 597 Menand, T., K. A. Daniels, and P. Benghiat (2010), Dyke propagation and sill formation in a
 598 compressive tectonic environment, *J. Geophys. Res.*, 115(B8), B08201.
 599 Mezger, T. G. (2002), *The Rheology Handbook: For Users of Rotational and Oscillatory Rheometers*.
 600 Michon, L., F. Saint-Ange, P. Bachelery, N. Villeneuve, and T. Staudacher (2007), Role of the
 601 structural inheritance of the oceanic lithosphere in the magmato-tectonic evolution of Piton de la
 602 Fournaise volcano (La Réunion Island), *J. Geophys. Res.*, 112(B4), B04205.

603 Nakamura, K. (1977), Volcanoes as possible indicators of tectonic stress orientation - principle and
 604 proposal, *Journal of Volcanology and Geothermal Research*, 2(1), 1-16.
 605 Ramberg, H. (1981), Deformation structures in theory and experiments, *Symposium on experiment
 606 and theory in geology*, 103(1), 131.
 607 Ranalli, G. (1995), *Rheology of the Earth*.
 608 Richards Jr, R., and R. Mark (1966), Gelatin models for photoelastic analysis of gravity structures -
 609 Paper describes a series of tests to show that body-force stress distributions can be conveniently
 610 found with gelatin models, *Experimental Mechanics*, 6(1), 30-38.
 611 Rivalta, E., and T. Dahm (2006), Acceleration of buoyancy-driven fractures and magmatic dikes
 612 beneath the free surface, *Geophysical Journal International*, 166(3), 1424-1439.
 613 Rodríguez, S. R., W. Morales-Barrera, P. Layer, and E. González-Mercado (2010), A quaternary
 614 monogenetic volcanic field in the Xalapa region, eastern Trans-Mexican volcanic belt: Geology,
 615 distribution and morphology of the volcanic vents, *Journal of Volcanology and Geothermal Research*,
 616 197(1-4), 149-166.
 617 Roman, D. C. (2005), Numerical models of volcanotectonic earthquake triggering on non-ideally
 618 oriented faults, *Geophys. Res. Lett.*, 32(2), L02304.
 619 Rooney, T. O., I. D. Bastow, and D. Keir (2011), Insights into extensional processes during magma
 620 assisted rifting: Evidence from aligned scoria cones, *Journal of Volcanology and Geothermal
 621 Research*, 201(1-4), 83-96.
 622 Roper, S. M., and J. R. Lister (2007), Buoyancy-driven crack propagation: The limit of large fracture
 623 toughness, *Journal of Fluid Mechanics*, 580, 359-380.
 624 Rubin, A. M. (1993), Tensile Fracture of Rock at High Confining Pressure: Implications for Dike
 625 Propagation, *J. Geophys. Res.*, 98.
 626 Rubin, A. M. (1995), Propagation of magma-filled cracks, *Annual Review of Earth & Planetary
 627 Sciences*, 23, 287-336.
 628 Shankar Subramanian, R. (1992), The motion of bubbles and drops in reduced gravity.
 629 Siebe, C., V. Rodríguez-Lara, P. Schaaf, and M. Abrams (2004), Radiocarbon ages of Holocene
 630 Pelado, Guespalapa and Chichinautzin scoria cones, south of Mexico city: Implications for
 631 archaeology and future hazards, *Bulletin of Volcanology*, 66(3), 203-225.
 632 Simakin, A., and A. Ghassemi (2010), The role of magma chamber-fault interaction in caldera forming
 633 eruptions, *Bulletin of Volcanology*, 72(1), 85-101.
 634 Stevenson, D. J. (1982), Migration of fluid-filled cracks: Applications to terrestrial and icy bodies,
 635 *Lunar Planet. Sci. Conf.*, 13, 768-769.
 636 Taisne, B., and S. Tait (2009), Eruption versus intrusion? arrest of propagation of constant volume,
 637 buoyant, liquid-filled cracks in an elastic, brittle host, *Journal of Geophysical Research B: Solid Earth*,
 638 114(6).
 639 Taisne, B., and C. Jaupart (2009), Dike propagation through layered rocks, *J. Geophys. Res.*, 114(B9),
 640 B09203.
 641 Taisne, B., and S. Tait (2011), Effect of solidification on a propagating dike, *J. Geophys. Res.*, 116(B1),
 642 B01206.
 643 Taisne, B., S. Tait, and C. Jaupart (2011a), Conditions for the arrest of a vertical propagating dyke,
 644 *Bulletin of Volcanology*, 73(2), 191-204.
 645 Taisne, B., F. Brenguier, N. M. Shapiro, and V. Ferrazzini (2011b), Imaging the dynamics of magma
 646 propagation using radiated seismic intensity, *Geophys. Res. Lett.*, 38(4), L04304.
 647 Takada, A. (1990), Experimental study on propagation of liquid-filled crack in gelatin: shape and
 648 velocity in hydrostatic stress condition, *Journal of Geophysical Research*, 95(B6), 8471-8481.
 649 Takada, A. (1994), The influence of regional stress and magmatic input on styles of monogenetic and
 650 polygenetic volcanism, *Journal of Geophysical Research*, 99(B7), 13563-13573.
 651 Timoshenko, S. P., and J. N. Goodier (1970), *Theory of Elasticity*.
 652 Turcotte, D. L., and G. Schubert (1982), *Geodynamics: Applications of Continuum Physics to
 653 Geological Problems*.

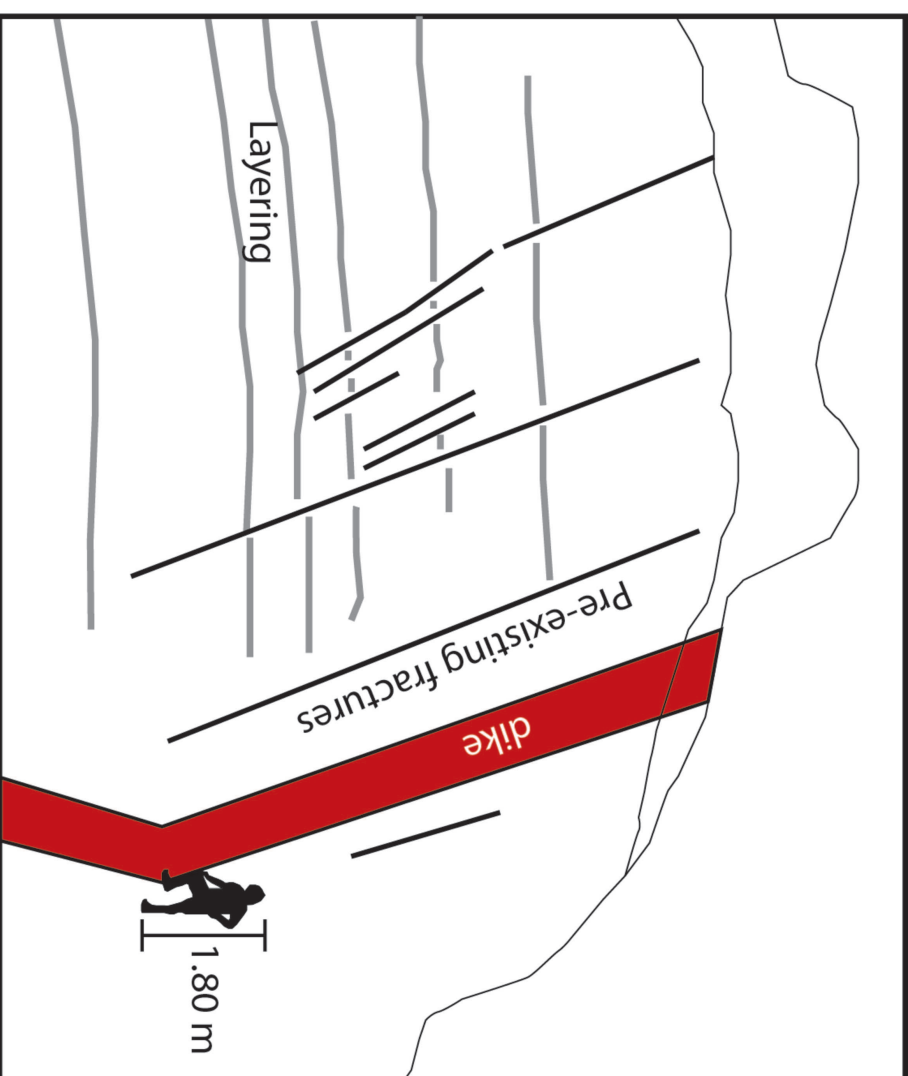
654 Valentine, G. A., and K. E. C. Krogh (2006), Emplacement of shallow dikes and sills beneath a small
655 basaltic volcanic center - The role of pre-existing structure (Paiute Ridge, southern Nevada, USA),
656 *Earth and Planetary Science Letters*, 246(3-4), 217-230.

657 Valentine, G. A., and N. Hirano (2010), Mechanisms of low-flux intraplate volcanic fields--Basin and
658 Range (North America) and northwest Pacific Ocean, *Geology*, 38(1), 55-58.

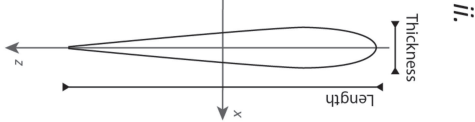
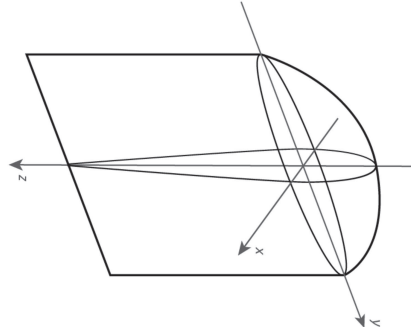
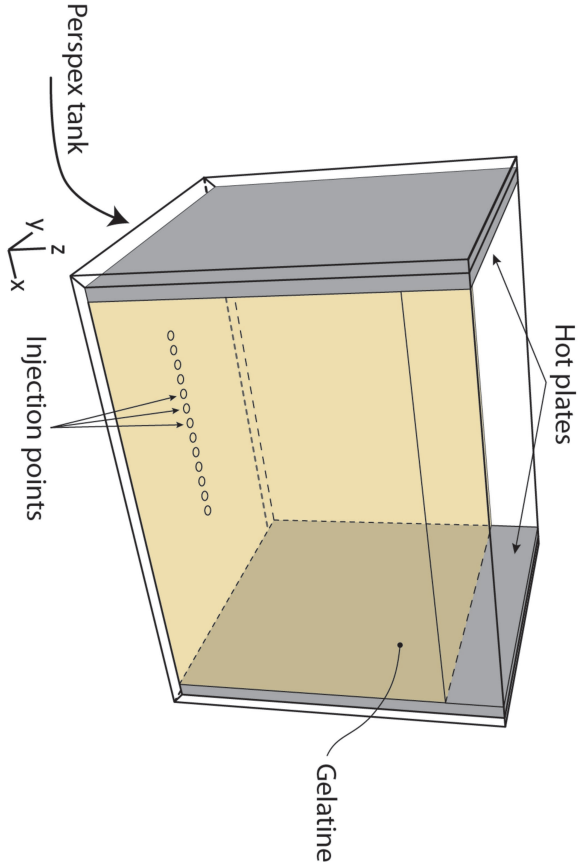
659 Wetmore, P. H., C. B. Connor, S. E. Kruse, S. Callihan, G. Pignotta, C. Stremtan, and A. Burke (2009),
660 Geometry of the Trachyte Mesa intrusion, Henry Mountains, Utah: Implications for the
661 emplacement of small melt volumes into the upper crust, *Geochem. Geophys. Geosyst.*, 10(8),
662 Q08006.

663 Zellmer, G. F., and C. Annen (2008), An introduction to magma dynamics, *Geological Society, London,*
664 *Special Publications*, 304(1), 1-13.

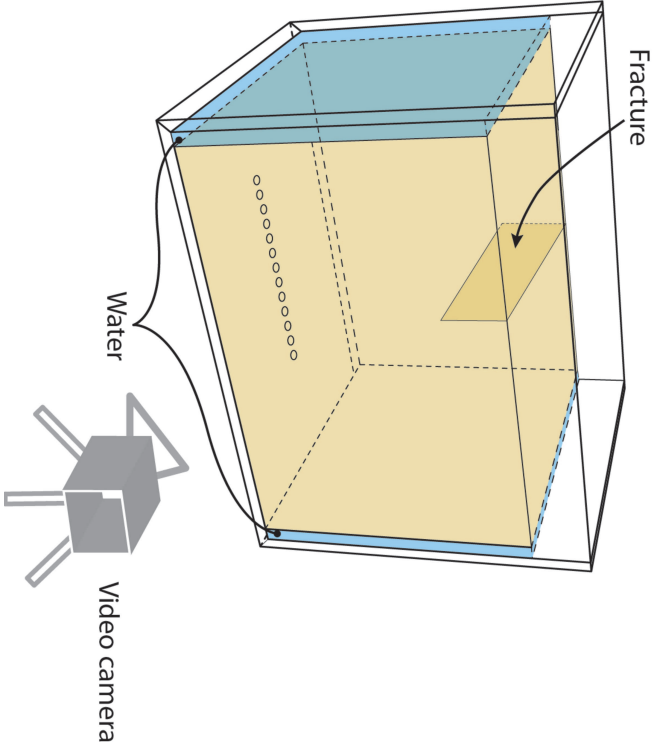
665 Ziv, A., A. M. Rubin, and A. Agnon (2000), Stability of dike intrusion along preexisting fractures,
666 *Journal of Geophysical Research B: Solid Earth*, 105(B3), 5947-5961.



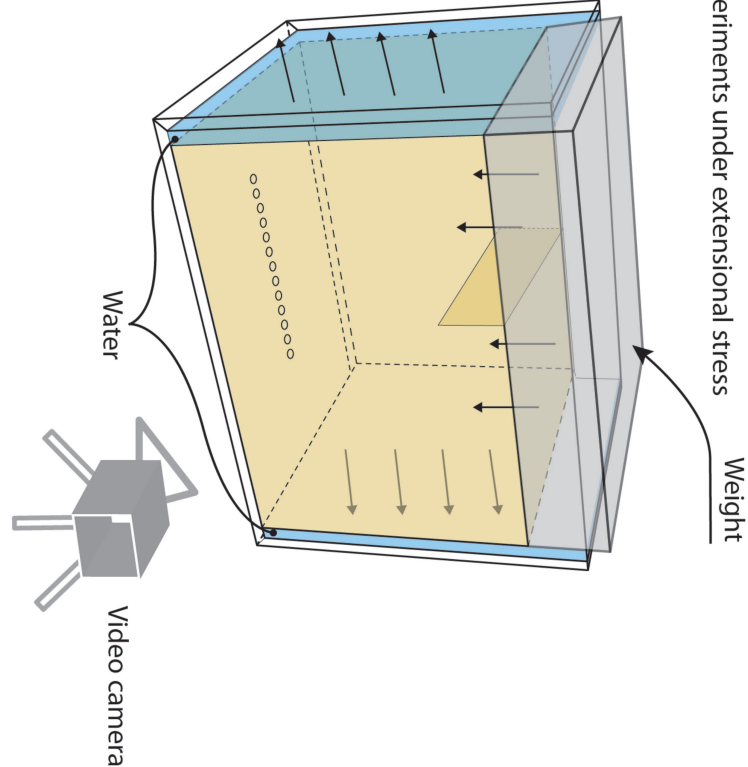
a. General setting

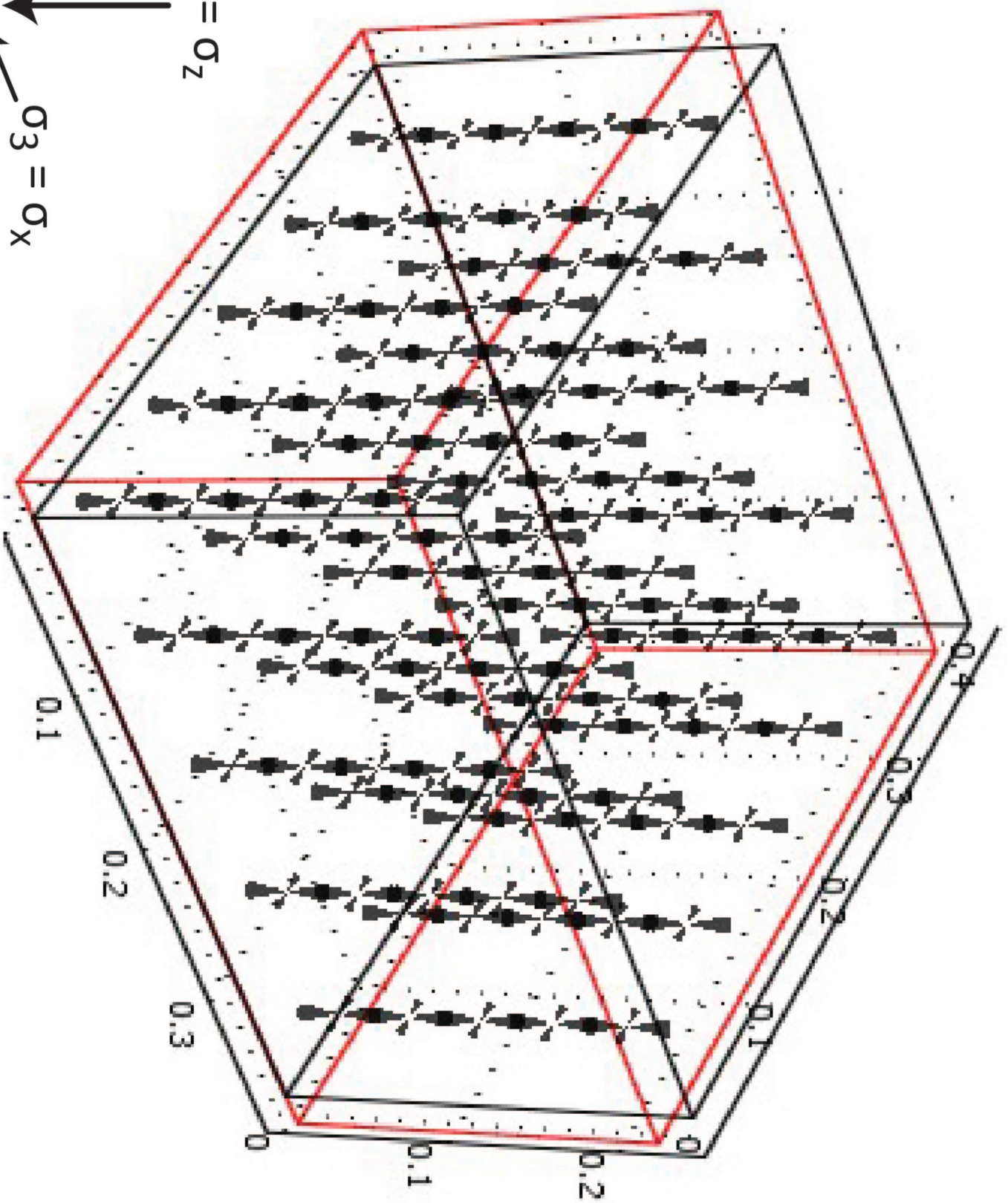


b. Experiments under hydrostatic stress



c. Experiments under extensional stress

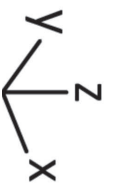




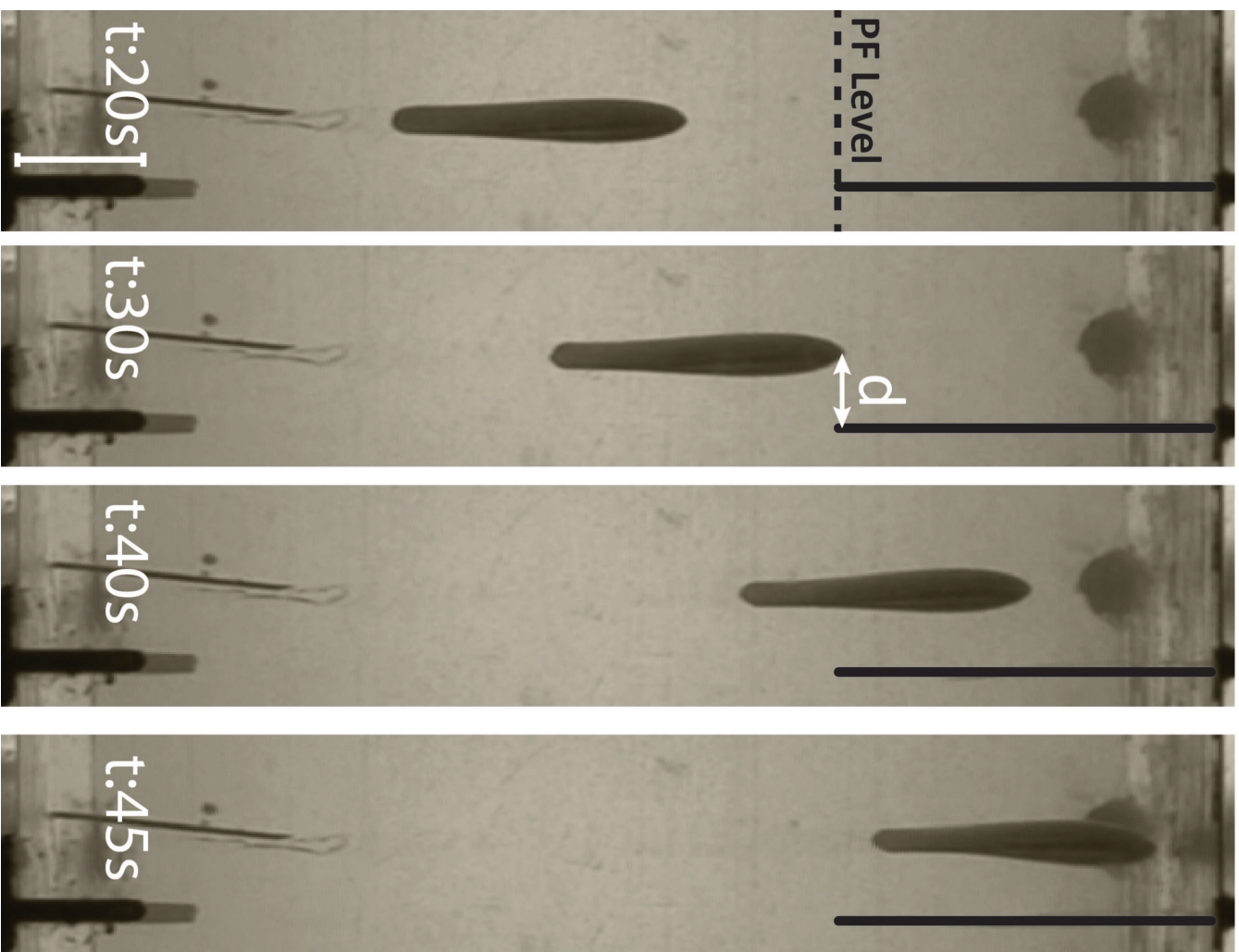
$$\sigma_1 = \sigma_z$$

$$\sigma_2 = \sigma_y$$

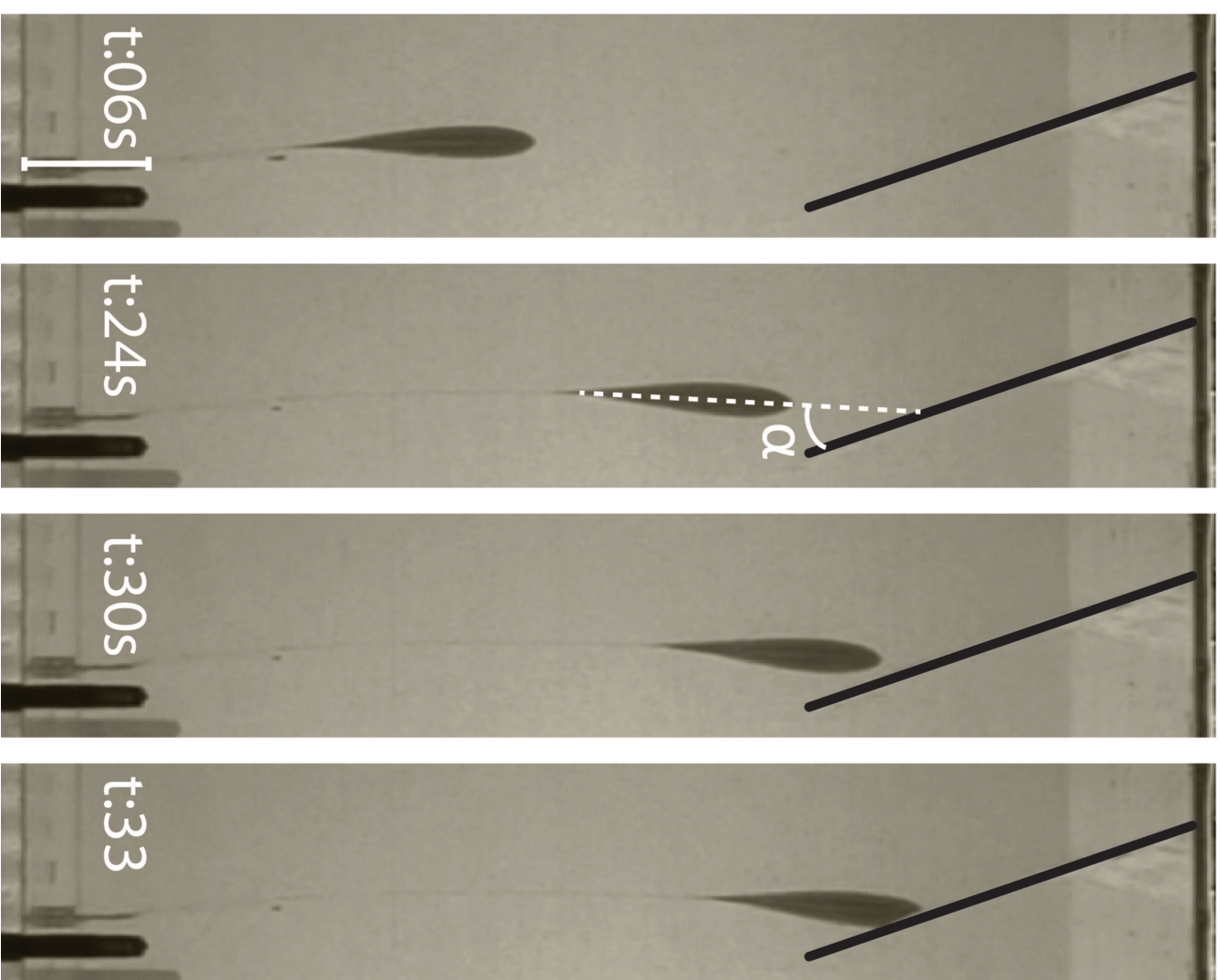
$$\sigma_3 = \sigma_x$$



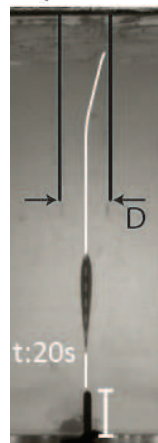
a.



b.



exp 3000



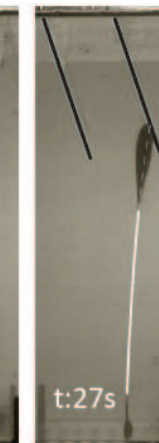
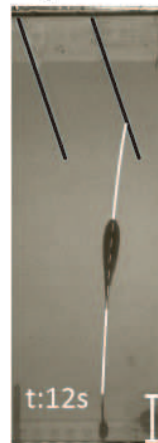
Change in direction

exp 2500



Change in direction

exp 2804L

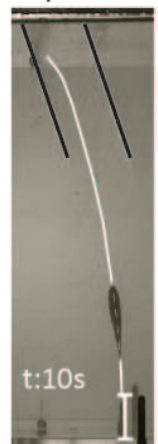


exp 2900



Change in direction

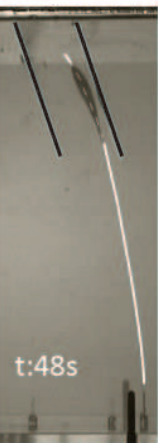
exp 2809R



Change in direction

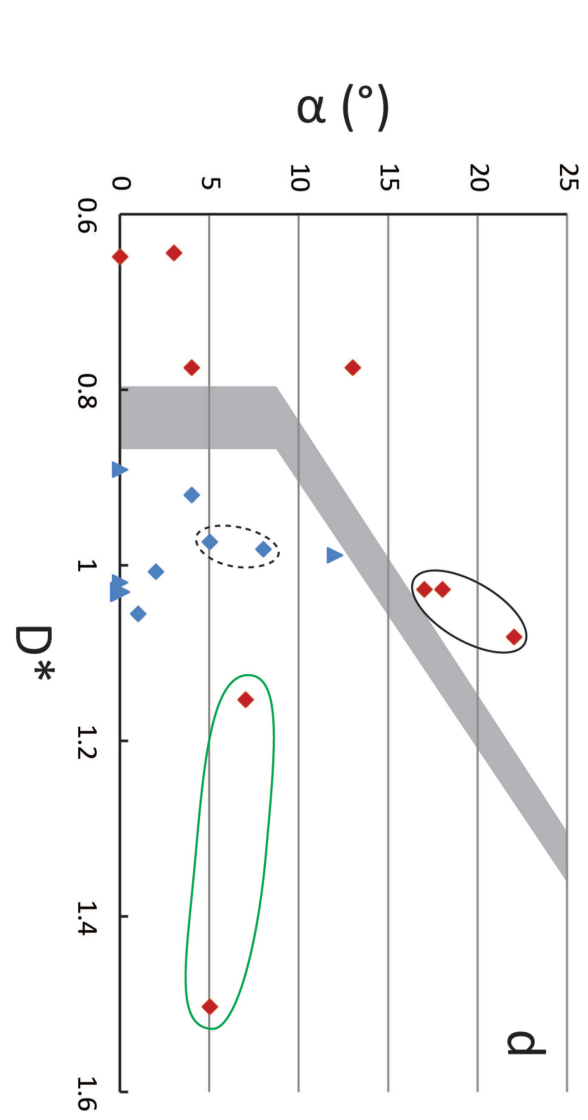
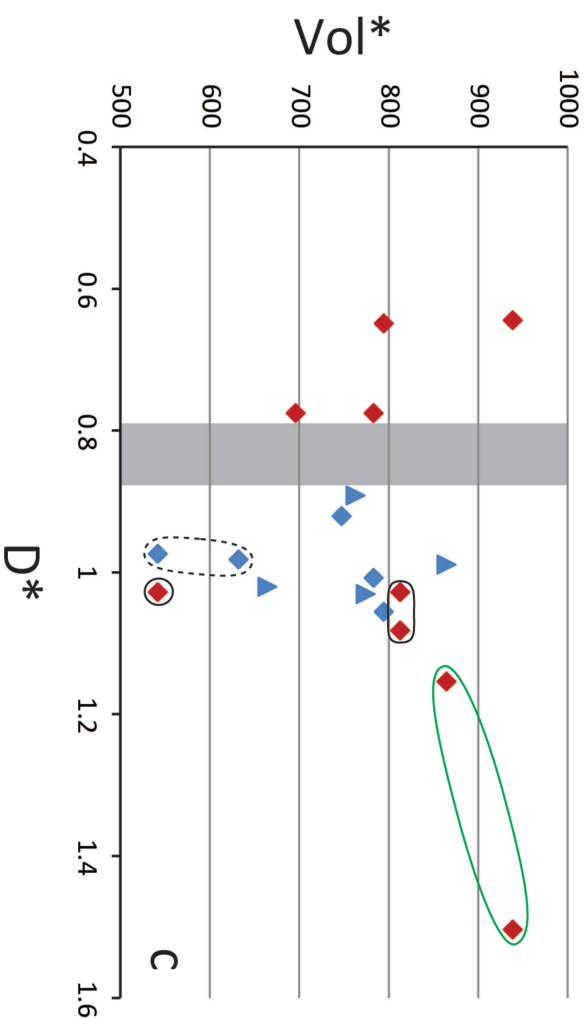
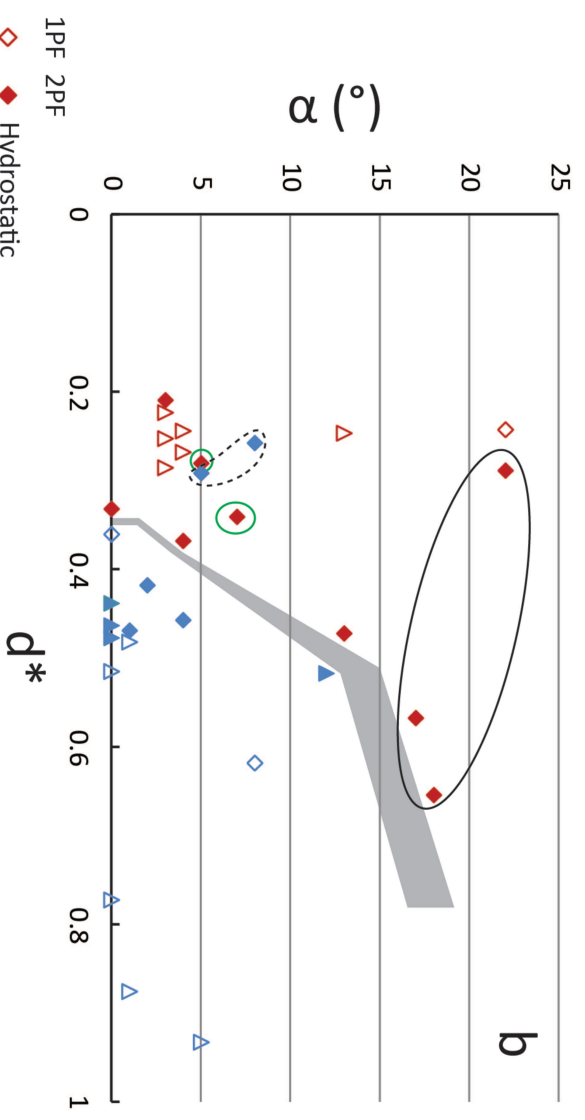
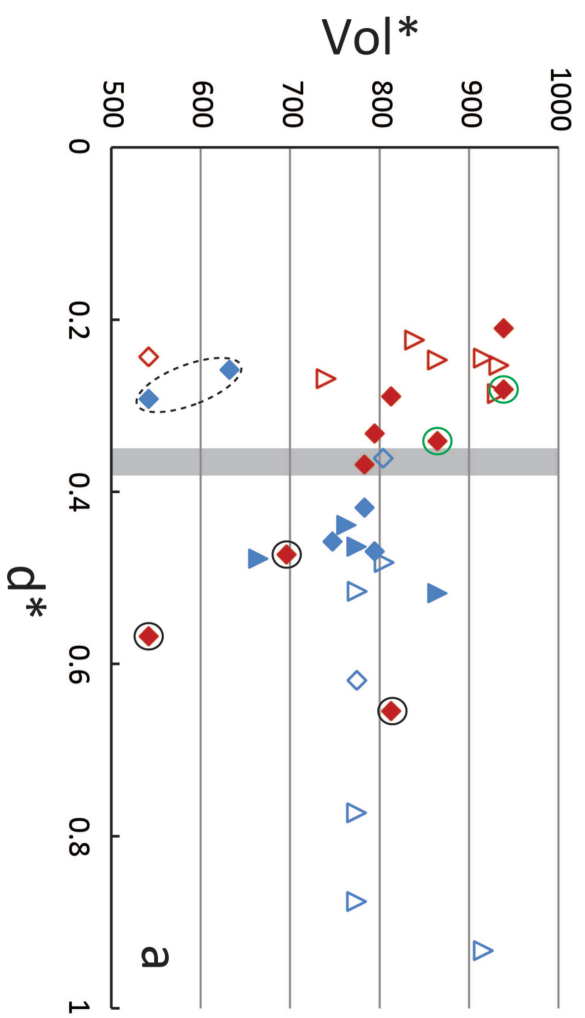
Propagation parallel to fractures

exp 2811R



Change in direction

Propagation parallel to fractures



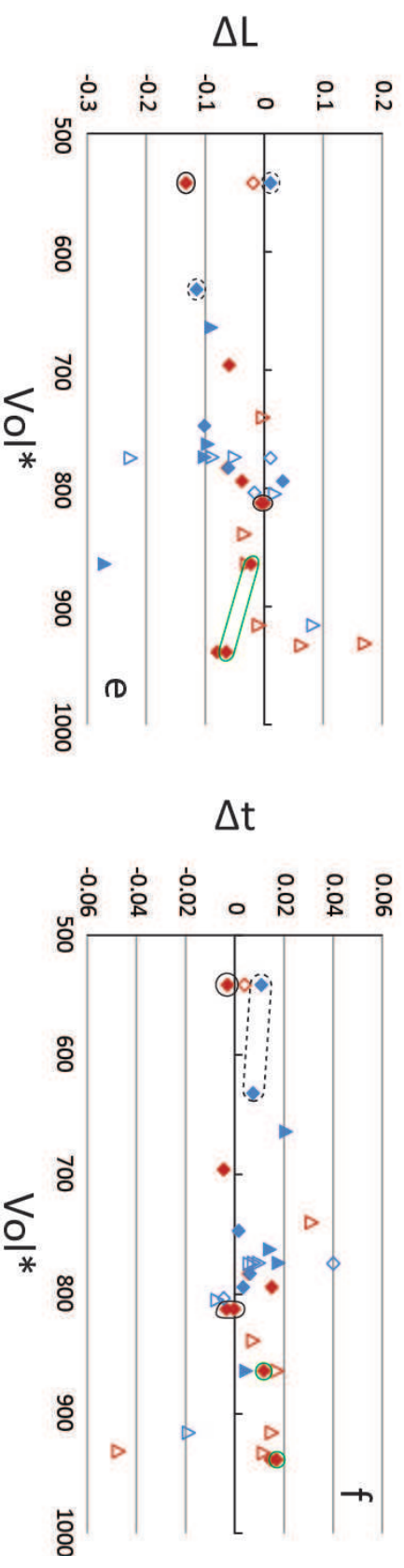
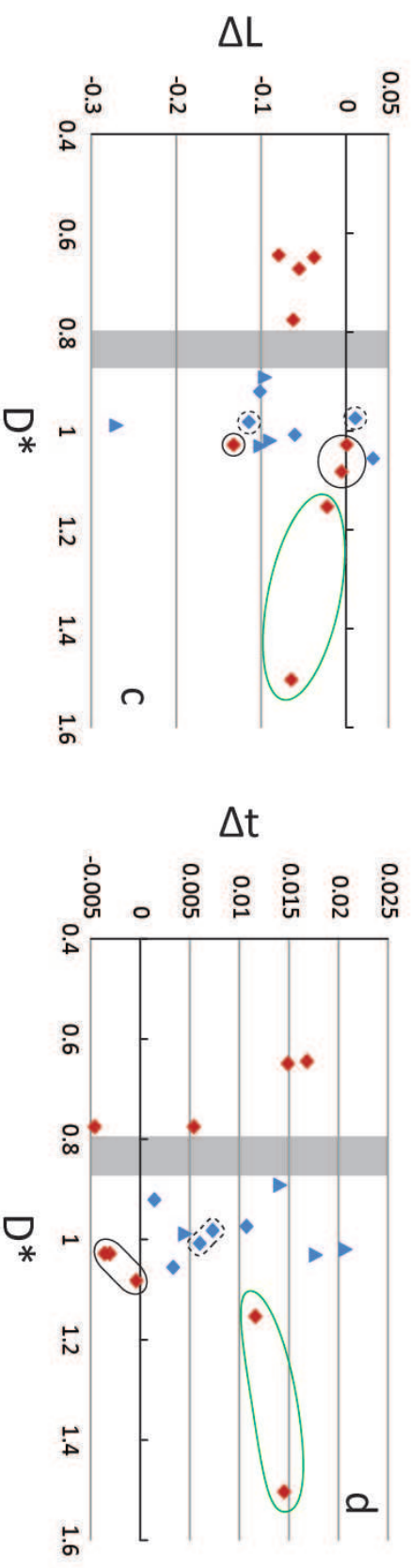
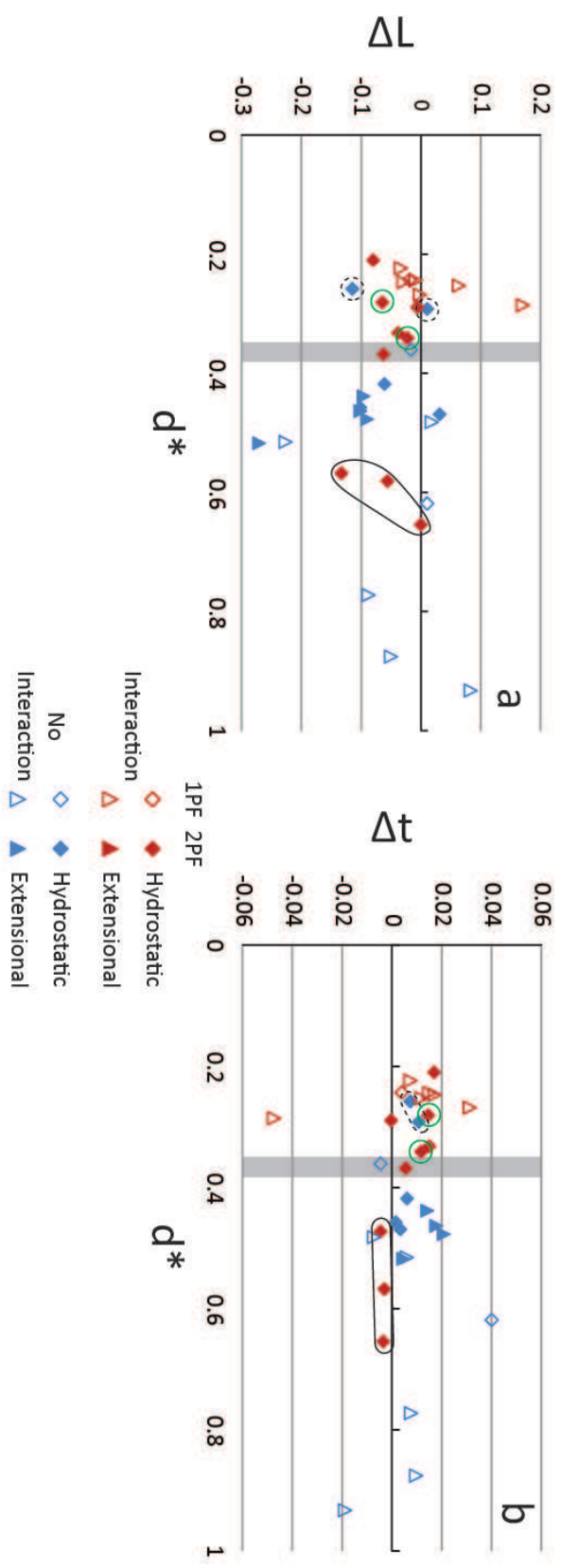
1PF 2PF

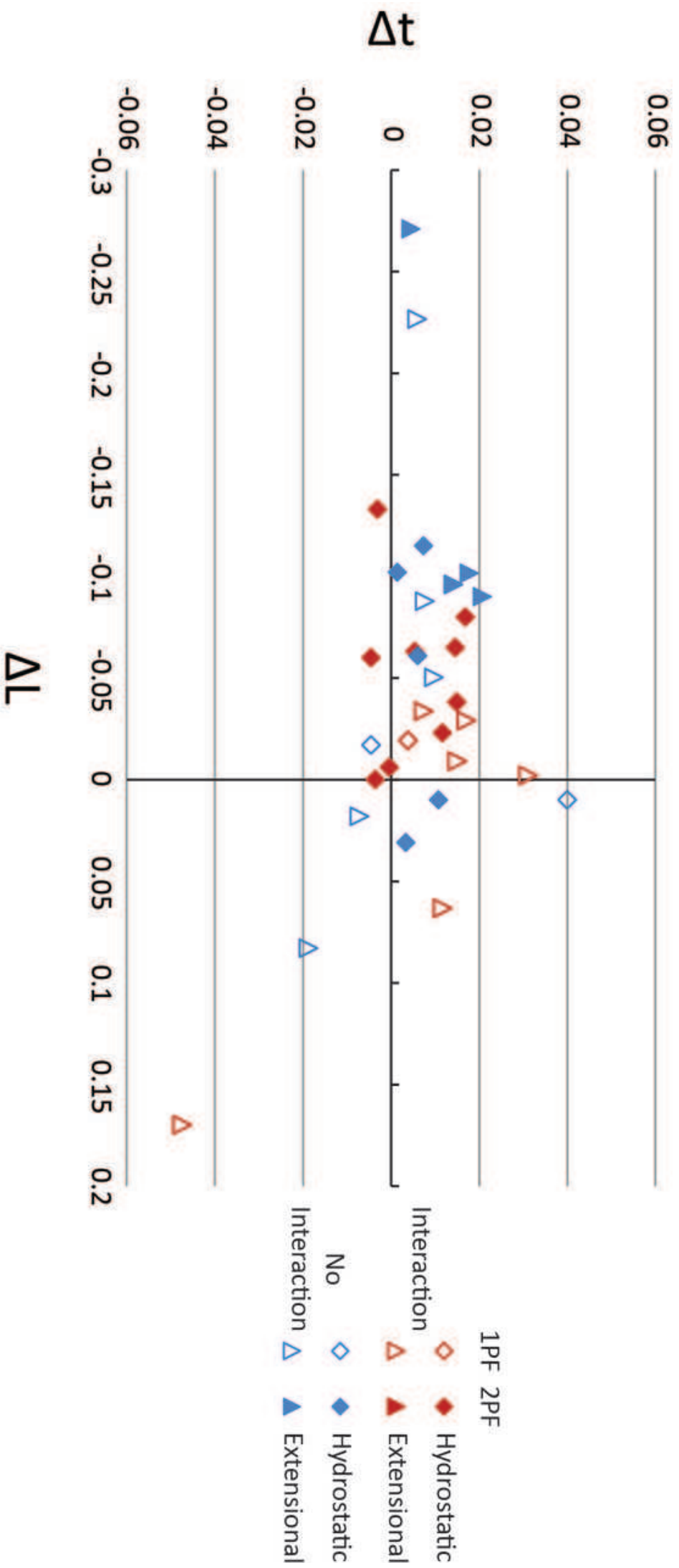
Interaction No

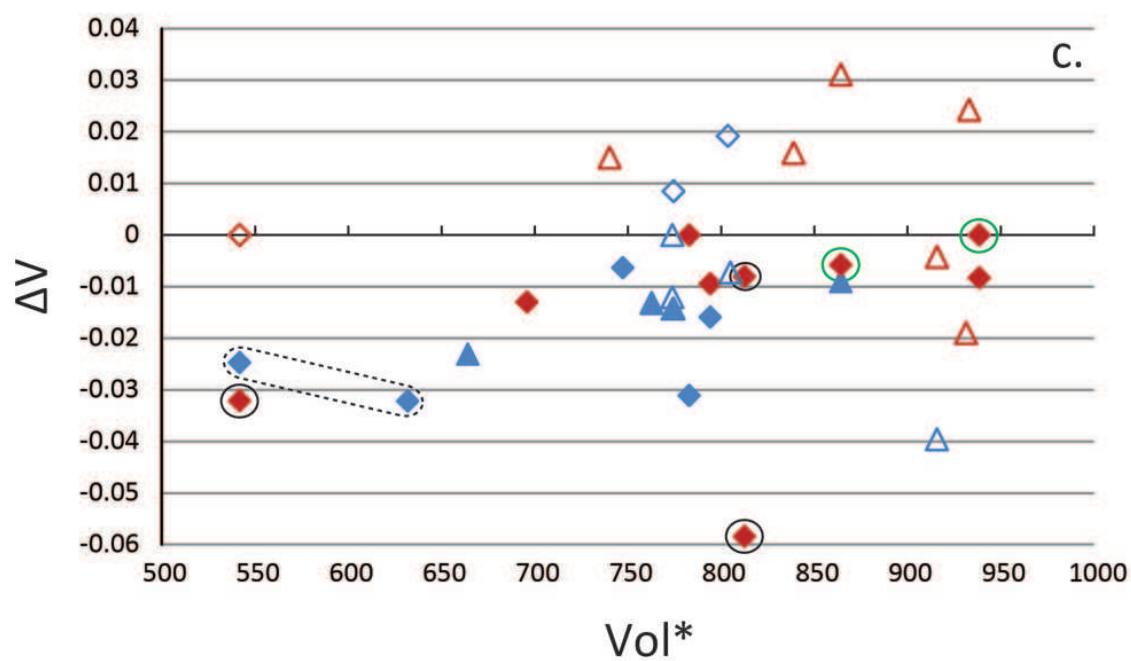
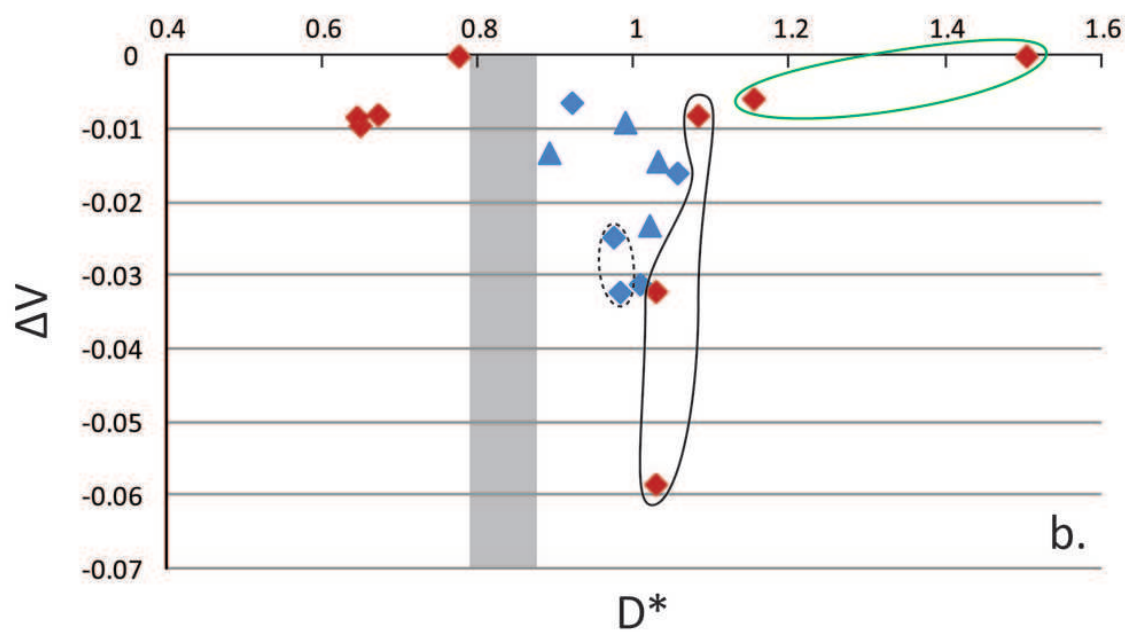
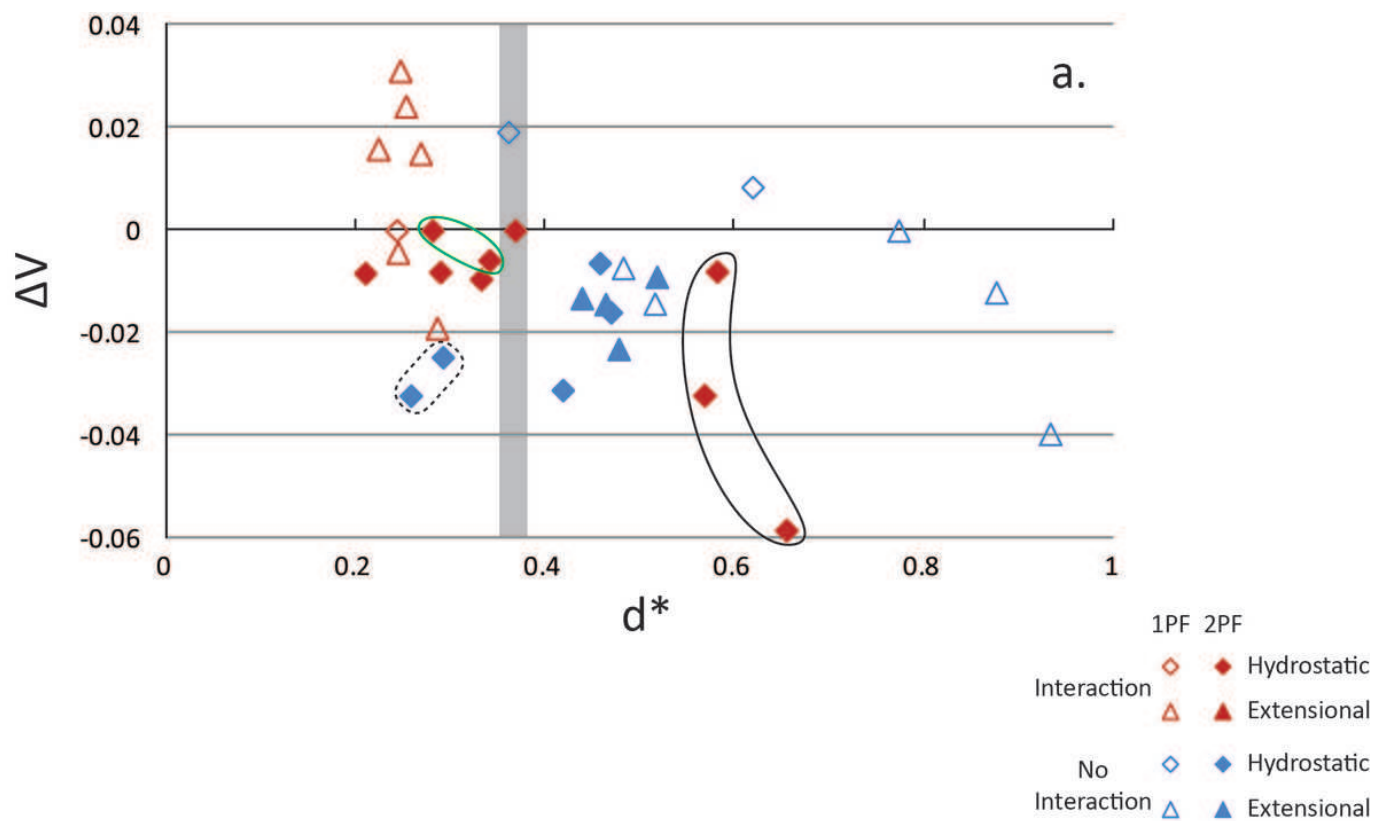
Interaction

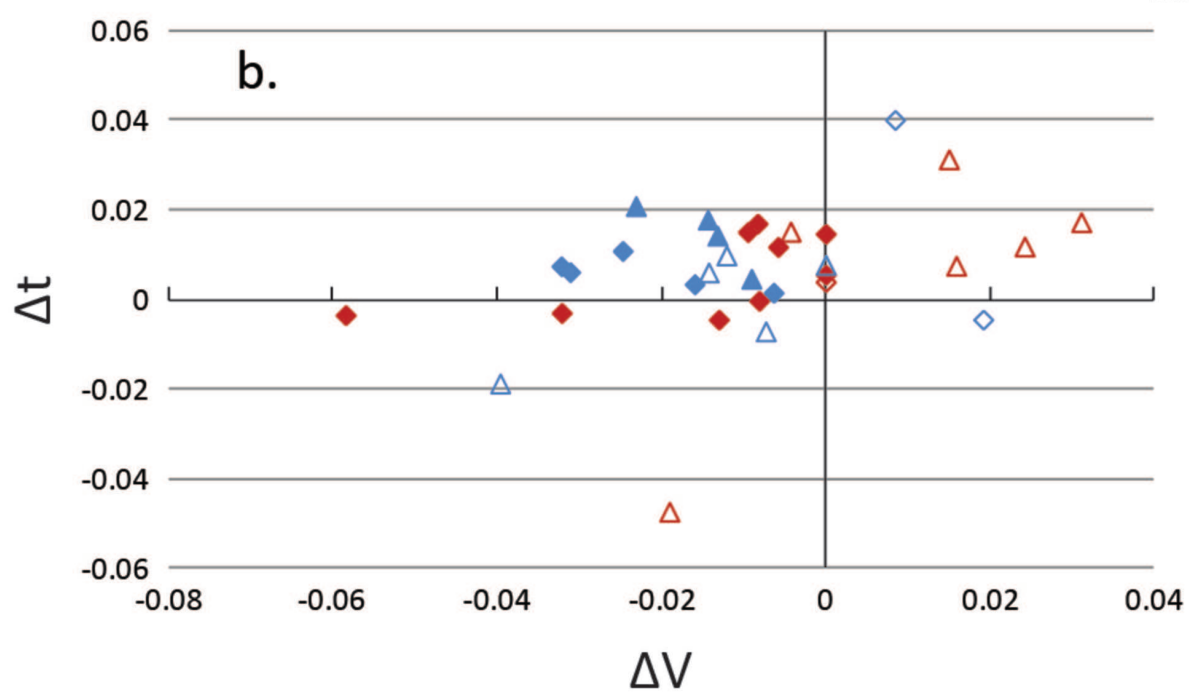
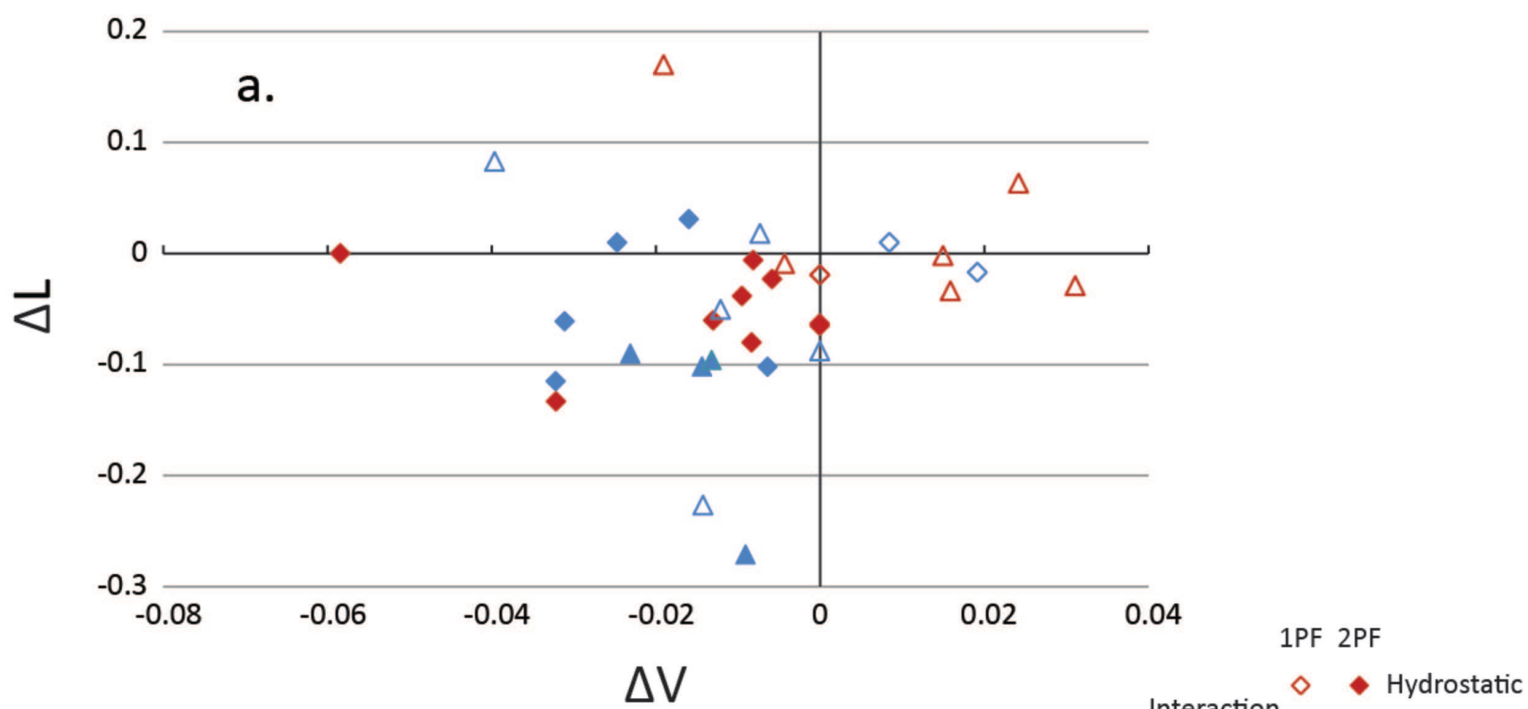
Hydrostatic

Extensional









1 Table 1

Volcanic fields	Minimum erupted volume (km ³)	Maximum erupted volume (km ³)	References
Abu, Japan	$3 \cdot 10^{-4}$	$5.94 \cdot 10^{-1}$	[Kiyosugi et al., 2009]
Auckland, New Zealand	$1.30 \cdot 10^{-5}$	2.39	[Allen and Smith, 1994]
Jeju, South Korea	$1.14 \cdot 10^{-4}$	$3.44 \cdot 10^{-1}$	[Hasenaka et al., 1997]
Chichinautzin, Mexico	$5 \cdot 10^{-4}$	$1.70 \cdot 10^{-1}$	[Siebe et al., 2004]
Mt. Etna, Italy	$2.72 \cdot 10^{-5}$	$4 \cdot 10^{-2}$	[Favalli et al., 2009]
Xalapa, Mexico	$1.40 \cdot 10^{-3}$	1.17	[Rodríguez et al., 2010]
Mean erupted volume (km ³)	$3.92 \cdot 10^{-4}$	$7.85 \cdot 10^{-1}$	

2

1 Table 2

Model		Lb*	Nature	
Gelatin height (m)	0.22 - 0.245	10^{-4}	2200 - 2450	Crustal thickness (m)
Gelatin length (m)	0.376 - 0.4		3760 - 4000	Crustal length (m)
Slit depth (m)	0.08 - 0.1		800 - 1000	Pre-existing fracture depth (m)
Slit length (m)	0.4		4000	Pre-existing fracture length (m)
Injected volume (ml)	8 - 11		$8 \cdot 10^{-3} - 1 \cdot 10^{-2}$	Injected volume (km ³)

2

1 Table 3

Experiments		E	Lb (m)	K_c (Pa.m ^{1/2})	PF	D (m)	D*	Volume injected (L)	Vol*	stress (Pa)
2PF Extension	2400	2869	0.0388	75	straight	0.04	1.03	0.009	774	203
	2600	3187	0.0402	79	straight	0.041	1.02	0.008	664	226
	2700	4111	0.0437	90	straight	0.039	0.89	0.01	763	166
	2900	3761	0.0425	86	angular (78°)	0.042	0.99	0.011	864	213
2PF Hydrostatic	2500	2869	0.0387	75	straight	0.039	1.01	0.009	783	0
	2512L	2869	0.0387	75	straight	0.03	0.78	0.008	696	0
	2504L	2869	0.0387	75	straight	0.03	0.78	0.009	783	0
	2609R	3187	0.0402	79	angular (81°)	0.037	0.92	0.009	747	0
	2800	2479	0.0370	70	angular (73°)	0.038	1.03	0.009	813	0
	2811R	2479	0.0370	70	angular (73°)	0.0363	0.98	0.007	632	0
	2804L	2479	0.0370	70	angular (73°)	0.04	1.08	0.009	813	0
	2804R	2479	0.0370	70	angular (73°)	0.038	1.03	0.006	542	0
	2809R	2479	0.0370	70	angular (73°)	0.036	0.97	0.006	542	0
	2909R	3761	0.0425	86	straight	0.049	1.15	0.011	864	0
	3000	4848	0.0462	97	straight	0.03	0.65	0.011	794	0
	3003L	4848	0.0462	97	straight	0.0298	0.64	0.013	938	0
	3004R	4848	0.0462	97	straight	0.0488	1.06	0.011	794	0
	3009R	4848	0.0462	97	straight	0.0695	1.50	0.013	938	0
1 PF Hydrostatic	1902L	3514	0.0415	83	straight	NaN	NaN	0.01	804	0
	2104R	2862	0.0388	75	straight	NaN	NaN	0.009	775	0
	2811L	2479	0.0370	70	angular (73°)	NaN	NaN	0.006	542	0
1 PF Extension	2002L	2551	0.0373	71	straight	NaN	NaN	0.009	805	181
	2102L	2862	0.0388	75	straight	NaN	NaN	0.009	775	203
	2202L	2988	0.0393	77	straight	NaN	NaN	0.011	933	212
	2302L	3278	0.0406	80	straight	NaN	NaN	0.009	740	349
	2406L	2869	0.0388	75	straight	NaN	NaN	0.009	774	203
	2406R	2869	0.0388	75	straight	NaN	NaN	0.009	774	203
	2704L	4111	0.0437	90	straight	NaN	NaN	0.011	839	166
	2903L	3761	0.0425	86	straight	NaN	NaN	0.011	864	213
	3100	4104	0.0437	90	straight	NaN	NaN	0.012	916	204
	3104R	4104	0.0437	90	straight	NaN	NaN	0.012	916	204
	3201R	3902	0.0430	87	straight	NaN	NaN	0.012	931	208
No PF Extension	2200	2988	0.0393	77	NaN	NaN	NaN	0.011	933	212
No PF Hydrostatic	0404L	2663	0.0379	72	NaN	NaN	NaN	0.008	705	0
	1911L	3514	0.0415	83	NaN	NaN	NaN	0.01	1	0
	2009R	2551	0.0373	71	NaN	NaN	NaN	0.009	0	0

1 Table 4

Experiments		V _b	V _a	ΔV	L _b	L _a	ΔL	t _b	t _a	Δt	α (°)	d (m)	d*	Interaction
2PF Extension	2400	0.09	0.079	-0.01435	1.014	0.9	-0.1016	0.2	0.2002	0.0177	0	0.018	0.464	NO
	2600	0.05	0.023	-0.0231	0.9905	0.9	-0.09	0.1	0.1678	0.0207	0	0.0192	0.478	NO
	2700	0.04	0.026	-0.01319	1.102	1	-0.096	0.1	0.1527	0.0141	0	0.0192	0.439	NO
	2900	0.05	0.043	-0.00904	1.357	1.1	-0.271	0.2	0.1627	0.0045	12	0.022	0.518	NO
2PF Hydrostatic	2500	0.15	0.121	-0.0311	1.11	1	-0.061	0.2	0.205	0.006	2	0.0162	0.419	NO
	2512L	0.1	0.087	-0.013	1.13	1.1	-0.06	0.2	0.1669	-0.0046	13	0.0183	0.473	YES
	2504L	0.14	0.14	0	1.124	1.1	-0.063	0.2	0.1931	0.0054	4	0.01426	0.369	YES
	2609R	0.08	0.07	-0.00635	1.423	1.3	-0.102	0.2	0.1692	0.0014	4	0.0184	0.458	NO
	2800	0.15	0.088	-0.05841	0.9856	1	0	0.2	0.1983	-0.0036	18	0.0242	0.655	YES
	2811R	0.07	0.041	-0.03218	1.213	1.1	-0.115	0.2	0.1807	0.0073	8	0.00955	0.258	NO
	2804L	0.2	0.192	-0.0081	1.135	1.1	-0.006	0.2	0.2278	-0.0004	22	0.0107	0.290	YES
	2804R	0.09	0.061	-0.03212	1.258	1.1	-0.133	1.2	1.1925	-0.0031	17	0.021	0.568	YES
	2809R	0.05	0.024	-0.0247	1.049	1.1	0.01	0.2	0.1815	0.0107	5	0.0108	0.292	NO
	2909R	0.06	0.055	-0.00581	1.1448	1.1	-0.023	0.1	0.1582	0.0116	7	0.0145	0.341	YES
	3000	0.03	0.018	-0.00948	0.9963	1	-0.0381	0.1	0.1365	0.0149	0	0.01537	0.333	YES
	3003L	0.04	0.032	-0.00831	1.103	1	-0.08	0.1	0.1416	0.0168	3	0.00972	0.210	YES
	3004R	0.03	0.016	-0.01595	1.048	1.1	0.031	0.1	0.1232	0.0033	1	0.0217	0.469	NO
	3009R	0.03	0.033	0	1.133	1.1	-0.065	0.1	0.1292	0.0145	5	0.013	0.281	YES
1 PF Hydrostatic	1902L	0.07	0.087	0.01916	1.514	1.5	-0.017	0.2	0.1932	-0.0046	0	0.015	0.361	NO
	2104R	0.09	0.102	0.00844	1.117	1.1	0.01	0.2	0.2433	0.0399	8	0.024	0.619	NO
	2811L	0.63	0.63	0	1.008	1	-0.0192	0.1	0.1528	0.0038	22	0.009	0.244	YES
1 PF Extension	2002L	0.12	0.109	-0.0073	1.045	1.1	0.018	0.2	0.2134	-0.0072	1	0.018	0.482	NO
	2102L	0.07	0.057	-0.01425	1.209	1	-0.2266	0.2	0.2066	0.0059	0	0.02	0.516	NO
	2202L	0.11	0.136	0.0242	0.8783	0.9	0.0633	0.2	0.1992	0.0117	3	0.00996	0.253	YES
	2302L	0.1	0.112	0.01499	0.8455	0.8	-0.002	0.2	0.2545	0.0311	4	0.0109	0.269	YES
	2406L	0.06	0.057	0	0.9313	0.8	-0.0877	0.2	0.1595	0.0076	0	0.03	0.773	NO
	2406R	0.06	0.044	-0.01208	1.013	1	-0.0503	0.2	0.1782	0.0097	1	0.034	0.876	NO
	2704L	0.04	0.056	0.01588	1.029	1	-0.0337	0.1	0.1526	0.0074	3	0.0098	0.224	YES
	2903L	0.04	0.075	0.03109	1.086	1.1	-0.029	0.2	0.1683	0.0171	13	0.0105	0.247	YES
	3100	0.07	0.065	-0.00428	0.9522	0.9	-0.009	0.2	0.1685	0.015	4	0.0107	0.245	YES
	3104R	0.06	0.024	-0.03962	1.002	1.1	0.083	0.2	0.1507	-0.0188	5	0.0408	0.933	NO
	3201R	0.06	0.043	-0.01903	1.214	1.4	0.17	0.3	0.2157	-0.0474	3	0.0123	0.286	YES
No PF Extension	2200	0.1	0.097	0	0.9737	1	0	0.2	0.178	0	0	NaN	NaN	NaN
No PF Hydrostatic	0404L	0.04	0.038	0	1.187	1.2	0	0.1	0.1286	0	0	NaN	NaN	NaN
	1911L	0.06	0.055	0	1.4	1.4	0	0.1	0.1494	0	0	NaN	NaN	NaN
	2009R	0.09	0.092	0	1.2	1.2	0	0.2	0.181	0	0	NaN	NaN	NaN

